A Dissertation
Presented to
The Academic Faculty

by

Benton R. Jaco

In Partial Fulfillment
of the Requirements for the Degree
Master of Science in the
School of Biological Sciences

Georgia Institute of Technology
May 2025

METABOLOMIC ANALYSIS OF PREDATOR URINE FOR ENHANCING OYSTER SHELL STRENGTH AND ECOLOGICAL IMPLICATIONS

Approved by:

Dr. Julia Kubanek, Advisor
School of Chemistry and Biochemistry
Georgia Institute of Technology

Dr. Marc Weissburg
School of Biological Sciences
Georgia Institute of Technology

Dr. Facundo Fernendez
School of Chemistry and Biochemistry
Georgia Institute of Technology

Date Approved: December, 18, 2024

To my friends, family, colleagues and teachers.

ACKNOWLEDGEMENTS

Graduate school has been a journey of profound growth and intense challenges, with every year being enriching and demanding. Through it all, I learned more than I would have thought possible and have grown into someone I am deeply proud to be. I am tremendously grateful for this experience and the many people who have supported me during this period.

Firstly, I am immensely grateful to my advisor and my graduate committee. My advisor Dr. Julia Kubanek, has been unwaveringly committed to my education, always pushing me to aim higher and become more, Julia fostered my academic development and interpersonal growth more than anyone else. I want to thank Dr. Marc Weissburg and Dr. Facundo Fernandez for serving on my graduate committee.

Thank you, Joe, Morgan, and Hartwell, for welcoming me into your home during graduate school – it has been a delight. To my partner Kaylyn, your constant encouragement and steadfast belief in me was my harbor during the most turbulent times; thank you for standing by my side every step of the way. I would also like to recognize Dr. Janie Wulff, whose passion for marine biology and guidance reignited my own love for the ocean and its fascinating inhabitants. I am also grateful to Dr. Andrew Shantz, who encouraged me to apply to the NSF GRFP.

I sincerely appreciate the academic bastions of the Georgia Institute of Technology and Florida State University, two outstanding institutions I have been fortunate to attend. To the National Science Foundation, thank you for awarding me an NSF Fellowship, I would not have been able to start this journey without it. Finally, to The United States Navy, thank you for teaching me so many valuable life lessons, thank you for supporting my education, and thank you for safeguarding the country I hold dear.

To all my family, friends, and loved ones, past and present, your influences shaped me into the person I am today; thank you. I have carried each of you with me through this journey, and this achievement belongs to you all.

TABLE OF CONTENTS

LIST OF TABLES

2023). All concentrations, means, and standard deviations are listed µM. Samples for which the molecular ion peak height (at *m/z* 155.0816) was below the UPLC-MS signal-to-noise detection threshold (1.5) of approximately 0.07 nM are listed as zero

LIST OF FIGURES

LIST OF SYMBOLS AND ABBREVIATIONS

POC	particulate organic carbon
DOC	dissolved organic carbon
HABs	harmful algal blooms
MSX	multinucleated sphere unknown
ppt	parts per thousand
ppm	parts per million
UPLC-MS	ultrahigh-pressure liquid chromatography-mass spectrometry
PLS-R	partial least square regression
VIP	variable importance in projection
^{1}H NMR	proton nuclear magnetic resonance
MHz	megahertz
ES	excitation sculpting
O1	Residual water peak frequency
LC-MS	liquid-chromatography mass spectrometry
SPE	solid phase extraction
Min	minutes
L	Liter
mL	milliliter
µL	microliter
cm	centimeter
mm	millimeter
µm	nanometer
nM	nanomolar

SUMMARY

This thesis explores the role of metabolites in blue crab urine that enhance oyster shell strength, with downstream opportunity to address the ecological and economic challenges posed by declining oyster (*Crassostrea virginica*) populations in the Gulf of Mexico gulf oyster. Gulf oysters are essential to Gulf Coast ecosystems, providing water filtration, carbon sequestration, and coastal protection while supporting a significant industry. However, populations have declined by up to 85% due to overfishing, habitat loss, pollution, disease, predation, and climate change.

Using integrated spectroscopic analyses and database matching, along with oyster growth assays, the study identified a metabolite in blue crab urine that promotes oyster shell strengthening. The study focused on the metabolite most important for oyster shell strengthening based on prior partial least squares regression analysis of mass spectrometric metabolomic data. 3-(1-methyl-*1H*-imidazol-4-yl) propanoic acid was identified as the primary contributor to this effect, with structurally similar molecules, 3-(1-methyl-*1H*-imidazol-2-yl) propanoic acid and 3-(1-methyl-*1H*-imidazol-5-yl) propanoic acid observed in aquarium oyster growth assays to induce similar levels of shell strengthening. This generalized strengthening response reflects oysters' adaptive strategy as r-selected species, which respond broadly to predator-associated cues.

The findings suggest that applying these chemical cues in oyster hatcheries could help produce a robust oyster spat more resistant to predation. Additionally, the study highlights the increasing power of metabolomic techniques to identify natural products in complex biological samples. Future research should employ and enhance these methods to

enable the rapid identification of unknown compounds, which could be applied to conservation efforts to assist in the restoration of populations such as gulf oyster populations.

CHAPTER 1. INTRODUCTION

1.1 Gulf oyster: ecosystem services, economic value and role as carbon sink

The gulf oyster, *Crassostrea virginica*, is a key species that plays a critical role in maintaining gulf coastal ecosystems (Sanjeeva, R. 2008; Grabowski et al., 2012; Belgrad et al., 2021). These organisms' value relates to the ecosystem services they provide (Coen et al., 1999; Beck et al., 2011; Grabowski et al., 2012). As broadcast spawners, gulf oysters release their gametes directly into the water column, to be fertilized and become larvae. They remain suspended in the water column for two to three weeks feeding on marine microalgae. After this period, larvae settle onto a hard substrate and metamorphose into small oysters called spat. While larvae can settle on various substrates, they tend to settle preferentially on oyster shells compared to other substrates. This preference is driven by chemical cues released by mature oysters, which attract larvae and induce their settlement (Tamburri et al., 2007; Zimme-Faust & Tamburri, 1994; Bonar et al., 1990). This fosters the aggregation and expansion of oyster reefs and develops the reef structure that provides broadscale ecosystem services.

Oysters contribute ecosystem services through water filtration among other processes. As filter feeders, oysters comb through the water column for free-floating prey such as marine microalgae. Other indigestible particles are encountered in the process, such as bacteria, detritus, and sediment, which are packaged as pseudofeces and deposited on the sea floor (Jorgensen, 1996). An oyster with a dry weight of 1 g may filter up a volume of 0.17 m^3 per day - approximately 170 liters (Ehrich & Harris, 2015). This filtration

reduces suspended particle load, nitrogen, and phosphorus levels improving water quality (Dame et al., 1989).

Through filtration, oysters help fight climate change. Carbon dioxide (CO_2) is a greenhouse gas and a driver of global warming. Slightly more than one-quarter (26%) of global CO_2 emissions were absorbed into the ocean annually from 2013 to 2022 (Friedlingstein et al., 2023). Marine phototrophs use dissolved CO_2 during photosynthesis. In doing so, the dissolved inorganic carbon (CO_2) is contained in an organic form in the body of phototrophs. Their organic carbon may be broken into small particles through excretion or the breakdown of phototrophs' mass. Such small particles exist as particulate organic matter (POM) or dissolved organic carbon (DOC), which differ according to their size class (Hartnett, 2018). Both digestible and indigestible suspended organic carbon particles are captured during oyster filtration and are excreted as fecal pellets or pseudofeces, respectively (Track & Polk, 1996). These excreted packages are too dense to remain suspended in the water column and sink to the sea floor. Upon reaching the sea floor, they are buried in marine sediment, storing the organic carbon contained therein (Kaspar et al., 1996; Dame et al., 1989). This mechanism of carbon sequestration is significant for two reasons: (1) oyster marine microalga prey, existing at the lowest trophic level, has a net negative carbon footprint, and (2) sequestering nutrient-replete organic material is inherently carbon-negative (Locher et al., 2021). Oysters offer an additional mechanism of carbon sequestration by incorporating digested carbon into their shells as calcium carbonate (Jansen & van den Bogaart 2020).

The three-dimensional structure of an oyster reef is, in and of itself, ecologically important. Being robust, stable, and erosion-resistant, oyster reefs can withstand strong

hydrodynamic forces (Reidenbach et al., 2013). Such resistance dissipates wave energy that could otherwise contribute to wave-induced erosion. This function is essential in the areas oyster reefs inhabit, which are frequently the coastal regions most susceptible to storm surges and coastal erosion. This is particularly true on the Gulf Coast, which surrenders an average of 8.2 ± 4.4 m of shoreline per year (Morton et al., 2005). Such erosion may be reduced by up to 40% by oyster reef wave breaks (Scyphers et al., 2011). Thus, the oyster reef structure directly maintains the integrity of the gulf coastline.

The ecosystem services provided by such a structure is beneficial for many marine organisms. With nooks and crannies of various sizes, oyster reef structures provide a nursery habitat and shelter for many marine organisms (Coen et al., 1999). Small fish and marine invertebrates use these recesses as a sturdy shelter, which most predators cannot easily overcome (Zu et al., 2016). For the same reasons oyster reef structure is used as a nursery habitat for many charismatic and economically important species (Zu et al., 2016; Coen et al., 1999). Protected nursery habitats are necessary for many marine ecosystems and may be provided by coral, mangrove roots, rocky outcrops or various other geologic and organic means (Hutchings and Recher 1974; Turner 1977, Orth et al. 1984, Minello 1999). However, alternative structural protection is seldom featured in many of the areas where oysters reside. Mudflats, for example, have muddy bottoms and turbid water. The turbid water of mudflats precludes the growth of marine plants and corals due to poor water quality and limited sunlight (Flowers et al., 2024). As such, the protection provided by oyster reef structures is frequently irreplaceable by natural means in many of the locations where oyster reefs form.

The ecological importance of gulf oysters is mirrored by their monetary value, persisting as a primary driver of Gulf Coast economies since the late 1800s (Edwin & Berrigan, 1997). The gulf oyster industry is precious to Gulf Coast communities, which produced an annual average of 15.7 million pounds of oyster meat since 2010, with an annual average value of $84.7 million National Marine Fisheries Service, 2024). Oyster shell is another valuable export used to produce lime, supplement animal feed, and for landscaping (Horiguchi et al., 2021; Lee et al., 2010; Aletor & Onibi, 1990). The Gulf Coast fishing industry, reliant on many species that require oyster reef nursery habitat, supports more than 60,000 jobs (Gordon et al., 2011). Oyster population trends are reflected in annual gulf oyster sales, decreasing from $93.6 million in 2019 to $62.2 million in 2020 (The National Marine Fisheries Service, 2024). Such economic benefits do not consider the apparent value of services such as shoreline stabilization or water filtration, which is less easily calculated. Despite this, such services are of clear economic value and could only be replaced through significant expense.

In summary, gulf oysters offer more than just a culinary delight; they are vital to the Gulf Coast ecosystem and economy. They serve as habitats for diverse species, protect coastlines from erosion, enhance water quality, and play a key role in combating climate change by sequestering carbon.

1.2 Gulf oyster population decline

1.2.1 Introduction

Oysters (*Crassostrea virginica*) are essential for maintaining Gulf Coast ecosystems. However, their population has severely declined in the last century, reduced by as much as

85% from historical levels (Zu Ermgassen et al., 2012; Beck et al., 2011). Many anthropogenic and natural factors have contributed to this decline (Mackenzie, 2007). Restoring oyster populations and the services they provide requires a comprehensive assessment of each contributing factor. This section will identify the significant drivers of this decline to establish the importance of identifying chemical cues that induce oysters to develop stronger shells.

1.2.2 Unsustainable Harvesting

Overfishing, driven by an increased demand for oysters as a food product, has been a major factor in the collapse of oyster populations along the Gulf Coast. Unsustainable harvesting practices have contributed to periods in which natural replacement rates are insufficient to sustain the population (Mann et al., 2009; Wilberg et al., 2011). This situation is exacerbated by a preference to harvest larger oysters, which are a more desirable food product but are also the primary reproductive individuals, producing more offspring than their smaller kin (Wilburg et al., 2011). As such unsustainable harvesting practices have diminished the abundance of oysters with the most reproductive potential and reduced the available substrate on which oyster larvae may settle.

1.2.3 Habitat Degradation

Habitat degradation is another contributor to the decline of oyster populations (Beck et al., 2011). Dredging and coastal development can directly damage oyster reef structure, causing large-scale oyster mortality. The damaged oyster reef structure further reduces the available substrate suitable for larval settlement (Nestlerode et al., 2007). Dredging also resuspends sediment which, despite oysters' ability to filter sediment from turbid waters,

can be damaging for several reasons. Larvae require a relatively clean substrate for settlement, and the deposition of sediment layers on the substrate precludes them from settling on such (Wilber & Clarke, 2010; Thomsen & McGlathery, 2006). High sediment loads overwhelm oysters' filtration mechanism, reducing their ability to feed. Sufficiently thick deposits of sediment, which can be more than a foot thick, may fill spaces in the reef structure marine organisms use for shelter (Buzan et al., 2015). Dredging may also expose fish to scavengers and opportunistic predators, which can reduce the total biodiversity and resiliency of the local ecosystem (Harrison, 1967; Thrush & Dayton 2002)

1.2.4 Water Quality Decline

Agricultural and urban runoff, as well as industrial pollution, lead to reduced water quality, negatively impacting oyster populations (Freeman et al., 2019). Runoff and pollution lead to eutrophication – excessively high nutrient levels. These nutrients, mainly nitrogen and phosphorus, are necessary for plant and marine microalgae growth (Smayda 2008). When present in excessive quantities, these nutrients can facilitate high rates of some marine microalgae growth, which may adversely affect oyster health (Thomsen & McGlathery, 2006).

Heavy metal contaminants are minor contributors to the decline of the oyster population. Studies have indicated that heavy metal accumulation in oyster tissues is variable across seasons and water conditions (Weng & Wang, 2019). The bioaccumulation of heavy metals in oyster tissue can contribute to population decline by reducing gonad quality (Weng & Wang, 2019; Volety, 2008). Thus, the effect of heavy metal pollution

may contribute to reduced reproductive capacity in heavily contaminated individuals and erode the population's capacity to absorb additional shocks.

1.2.5 Disease

Diseases such as dermo (*Perkinsus marinus)* and MSX (multinucleated sphere unknown, *Haplosporidium nelson)* cause significant mortality to gulf oyster populations during environmentally stressful periods (Burreson & Ragone Calvo, 1996).

1.2.6 Predation

Predation of oysters by blue crabs (*Callinectes sapidus*), oyster drills (*Urosalpinx cinerea*), and boring sponges (*Cliona celata*) is a contributing factor limiting oyster populations' ability to recover. These organisms prey heavily on young oysters, which have thinner shells, making them less well-defended against predation. Research shows that approximately 20% of juvenile mortality results from mesopredators (Carroll et al., 2015). While oyster populations have declined, the population of many of their predators has increased. This inverse trend in population growth has led to an increased predatory pressure for oysters (Booth et al., 2018). Predator population sizes have increased due to a loss of higher-level species that have historically acted to keep such populations in check (Mann & Powell, 2007). Water quality changes have introduced oyster drills and boring sponge predators into habitats previously protected by salinities incompatible with oyster drill physiology (Tice-Lewis et al., 2022). Such predator-prey interactions are further discussed in section 1.3 of this thesis.

1.2.7 Climate Change

As suggested previously, climate change has acted as a global amplifier of oyster stressors. Rising sea levels change tidal heights and shift intertidal oyster populations into subtidal regions (Bartol et al., 1999). Increased sea temperatures exacerbate the prevalence of diseases like Dermo and MSX while in tandem affecting oyster metabolic processes reducing growth and reproduction (Jerelle et al., 2020). Salinity changes, driven by shifting precipitation and freshwater influx patterns, have created suboptimal conditions for the survival of oysters (Scavia et al., 2002). Optimum salinity regimes for gulf oyster larvae are dependent on the salinity in which the gonads of the prior generation had developed, and the greater the difference between this and the salinity they develop in as larvae, the more suboptimal conditions are for their development (Davis, 1958).

1.2.8 Harmful Algal Blooms (HABs) and Toxins

Harmful algal blooms (HABs), such as those caused by *Karenia brevis*, *Dinophysis acuminata,* and *Alexandrium catenella* impact larval health. For example, *D. acuminata* causes mortality in oyster larvae at 1000 cells/ml, while exposure at any concentration to *D. acuminata* stops larval swimming or causes death (Pease et al., 2022). Upon bloom termination, algal decomposition results in hypoxic or anoxic areas, causing reduced metabolic function or death, respectively, for aerobic organisms (Anderson & Taylor, 2001). Reduced metabolic function due to hypoxic conditions can compromise oyster growth, reproduction, and immune function through the extend of the hypoxic event (Breitburg et al., 2018).

1.2.9 Leveraging Chemical Cues for Oyster Restoration

Some prey organisms respond to the threat of nearby predators with induced chemical defenses, altered behaviours, or changes to their morphology (Brönmark and Miner 1992; Cronin and Hay 1996; Baldwin 1998; Werner and Gilliam 2003; Schmitz 2008; Weissburg et al. 2016). These inducible responses enhance prey survival by mitigating the impact of predation (Lima 1998). Among the various sensory methods used to detect predators, chemosensation is particularly effective in environments where other senses are limited; chemical cues are often the main method of detecting predators in marine environments (Hay 2009).

Despite the recognized importance of chemical cues in shaping marine predator-prey dynamics and influencing marine ecosystem dynamics, few of the specific molecules enabling prey to detect their predators have been identified. Copepodamindes, from copepods, are detected by phytoplankton, which they use to assess the risk of predation and upregulate their toxicity in response (Selander et al., 2015; Selander et al., 2019). In freshwater systems, the phytoplankton *Scenedesmus subspicatus* are known to detect fatty-acid derivatives released from their *Daphnia* predator and undergo morphological adaptions to reduce *Daphnia* grazing (Hessen & van Donk., 1993; Yasumoto et al., 2005). Prior research on prey detection of blue crab predators, *Callinectes sapidus*, has shown that homarine and trigonelline, urinary components of the blue crab, suppress the foraging behavior of one important prey species, the mud crab, *Panopeus herbstii* (Weissburg et al., 2016; Poulin et al., 2018; Roney et al., 2023). Oysters, also prey of blue crabs, respond to these cues by growing thicker and stronger shells (Schrerer et al., 2016; Scherer et al., 2017). The induced strengthening of oysters shells is significantly beneficial to their

survival. After four weeks of exposure to predator cues, oyster spat have stronger shells and 58% increased survival compared to unexposed controls (Belgrad et al., 2023).

While homarine and trigonelline induce oyster shell strengthening, these cues were not identified as the most important cues for inducing oyster shell strengthening in blue crab urine (Cepeda, 2023). In that study, Cepeda determined that yet unidentified metabolites were more important in predicting the potency of blue crab urine to induce oyster shell strengthening. Identifying the chemical cues in blue crab urine most important for oyster shell strengthening could broadly benefit restoration efforts by incorporating them to cultivate more resilient oyster populations (Smee & Bellgrad., 2023). By identifying and leveraging these chemical cues restoration efforts will be better equipped to facilitate the recovery of oyster ecosystems.

1.2.10 Conclusion

Many factors, frequently compounding or additive in nature, drive the decline of gulf oyster populations. Anthropogenic factors, including unsustainable harvesting practices, water quality decline, and habitat degradation, can be partially or wholly mitigated by adapting human activity. Harmful algal blooms, disease, and climate change are natural forces exacerbated by anthropogenic factors. The remaining factor, predation, requires a more well-informed strategy to mitigate its impact on oysters. Such considerations have necessitated the research discussed in this thesis.

Prior research by Cepeda (2023) identified mass spectral features in blue crab urine associated with metabolites that are most important for inducing oyster shell strengthening.

The current research seeks to identify the molecular structures of the features identified by Cepeda and investigates the induction of such molecules in shell strengthening.

CHAPTER 2. METHODS

2.1 Prior Research: Bioassay and Metabolomic Analysis

Oyster (*Crassostrea virginica*) shell-strengthening assays were conducted by collaborators at Dauphin Island Sea Lab using blue crab urine mixtures using methods previously described (Roney et al., 2023; Cepeda, 2023). Oyster spat were exposed to treatments of blue crab (*Callinectes sapidus*) urine mixtures, homarine, trigonelline, predator water, and seawater control. Blue crab urine used in this assay was collected from blue crabs sourced from the Gulf of Mexico, fed a diet of oysters or mud crabs. The urine was combined into 24 unique urine mixtures – 12 from blue crabs fed oysters and 12 from blue crabs fed mud crabs. Each mixture was composed of urine from different crabs to ensure variety across urine treatments, with 3-12 individual blue crabs represented in each unique urine mixture. Predator water treatments consisted of water collected from blue crab holding tanks. Shell crushing force and oyster spat length were measured after eight weeks of exposure to one of the chemical treatments given above.

Blue crab urine samples were analyzed using hydrophilic interaction liquid chromatography (HILIC) ultrahigh-pressure liquid chromatography-mass spectrometry (UPLC-MS). Peaks were detected with a signal-to-noise (S/N) threshold of 1.5. Blue crab urine LC-MS data were used to generate partial least square regression (PLS-R) models correlating molecular features with shell strengthening. Genetic algorithm variable selection was used to refine the list of LC-MS features considered in the models, improving performance and reducing overfitting (Wold et al., 2001). Variable importance in projection (VIP) scores were calculated for each feature that correlated with shell

strengthening, and the ten features most important to the models were tabulated (Cepeda, 2023). The results in this thesis build on these prior results by pursuing the molecular structures of prioritized features most important for oyster shell strengthening as indicated by feature VIP scores.

2.2 Urine preparation and ^{1}H NMR spectral acquisition

Blue crab urine samples were prepared for ^{1}H nuclear magnetic resonance (NMR) spectral acquisition by combining 138 µL of urine, 46 µL sodium phosphate buffer solution (0.1 M, pH 7.4), 16 µL internal standard (0.1% 3-(trimethylsilyl)propanoic–2,2,3,3-d_4 acid (TMSP). Phosphate buffer and internal standard solutions were prepared in D_2O (99.9% atom D_2O; Sigma-Aldrich). Solutions were vortexed for 5 min, after which 175 µL was transferred to high-grade 3 mm NMR tubes (Wilmad Glass). Spectra were acquired with a Bruker Avance HD 800 MHz NMR spectrometer furnished with a 3 mm cryoprobe using a water suppression pulse with excitation sculpting (ES) for water suppression. Residual water peak frequency (O1) was identified using the ZGPR pulse sequence. Then, 128 spectral scans were acquired using the ZGESGP pulse sequence with water suppression centered on the identified O1.

2.3 Solid phase extraction of blue crab urine, urine extract preparation and ^{1}H NMR and 2D NMR spectral acquisition

A urine sample (BCO3) was selected for extraction and further NMR spectral analysis as it had the second highest relative concentration of ^{1}H NMR signals of interest, identified after normalizing ^{1}H NMR TMSP peak intensities across samples, and a sufficient sample volume was available, unlike BCO7 which had higher relative

concentration of ^{1}H NMR signals, but was not available in a sufficient quantity. Metabolites from urine sample BCO3 were concentrated by solid phase extraction (SPE) using an ENVI-18 SPE column (3 mL; 0.5 g). The SPE cartridge was attached upright to a vacuum manifold, primed with 1 mL LC-MS grade methanol, washed with 1 mL deionized H_2O. A 1 mL aliquot of urine was loaded onto the column, the column was washed with 1 mL deionized H_2O, and 1 mL LC-MS grade methanol was used to elute metabolites from the column. This eluate was portioned into two vials (90% for NMR spectral analysis; 10% for future LC-MS or other analysis), the solvent removed *in vacuo*, and the extracts stored at –20 °C. The extract assigned to NMR spectral analysis was dissolved in 128 µL D_2O and combined with 46 µL phosphate buffer (0.1 M in D_2O, pH 7.4), 16 µL TMSP internal standard, and vortexed for 5 min. Then, 175 µL of this mixture was transferred via micropipette to a 3 mm NMR tube (Norell Sample Vault Series (3 mm X 178 mm)).

A Bruker Avance HD 800 MHz NMR spectrometer with a 3 mm cryoprobe was used to acquire NMR and 2D NMR spectra of desalted urine extracts. ^{1}H NMR spectra were acquired in 128 scans using the ZGESGP pulse sequence. Homonuclear correlation spectroscopy (COSY) spectra were attained with 32 scans using a phase-sensitive Double Quantum Filtered COSY pulse sequence with Excitation Sculpting using 180 water-selective pulse and trim pulses (cosydfesgpphpp). Heteronuclear single quantum coherence (HSQC) spectra were collected with 180 scans in phase-sensitive mode with echo-antiecho and adiabatic pulses for inversion pulse sequence (hsqcetgpsp). Heteronuclear Multiple Bond Correlation (HMBC) spectra were acquired with 300 scans using a magnitude-mode presaturated pulse program with low-pass J-filter (hmbcgplpndqf).

2.4 NMR spectral processing and interpretation

Bruker TopSpin 4.3.0 was used to process and analyze ^{1}H NMR spectra. Spectra were calibrated by setting the TMSP peak to 0.0 ppm and manually phased. The chemical complexity of blue crab urine extracts created signal overlap that prevented the assignment of individual proton signals to particular metabolites . As such,^{1}H NMR spectral data were used to exclude particular candidate structures from consideration when experimental or predicted ^{1}H NMR spectral features were absent from urine extract spectra.

2.5 Identification of metabolites from NMR spectroscopic and MS data via database investigation and use of authentic chemical standards

The molecular formulae calculated by Cepeda (2023; Table 2) and MS^2 spectral peaks were searched in publicly available databases. Initial database searches were conducted using databases native to Compound Discoverer: MZCloud, Kegg, and ChemSpider. Additional databases compatible with Compound Discoverer were identified, imported and, searched including: LipidBlast-VS68-Neg, LipidBlast-VS68-Pos, EFS_Library, EFS_HRAM_Spectra_Library. Additional libraries, including MassBank, Global Natural Products Social Molecular Network (GNPS), and the National Institute of Standards and Technology (NIST), were searched manually. Manual searches were conducted with a 3 ppm mass error tolerance.

SIRIUS & CANOPUS (version 5.8.3) were used to propose candidate structures that may not have been included in spectral libraries. The mass spectral and tandem mass spectral data were exported as MZML files. These files were then imported into SIRIUS to predict molecular formulae and candidate molecular structures using CSI:FingerID. CSI:FingerID uses a machine learning model to predict molecular properties from MS^2

data, evaluates the similarity of the unknown compound to public databases, and generates a list of possible molecular structures. These were computed with the following parameter settings: Isotope pattern filtering, 3 ppm MS^2 mass accuracy, MS^2 isotopes were scored, and additional databases were searched during computation. The databases searched with SIRIUS were: Bio Database, Biocyc, CHEBI, COCONUT, EcoCycMine, GNPS, HMDB, HSDB, KEGG, KEGG Mine, KNApSAcK, Maconda, MeSH, NORMAN, Natural Products, Plantcyc, PubChem, PubMed, YMDB, YMDB Mine, and ZINC bio. Resultant database hits were prioritized if all the observed fragments matched database entries and if SIRIUS structural prediction scores were above 70%. Lower-priority candidate structures that did not meet these criteria were not pursued with authentic standards.

^{1}H NMR chemical shifts were predicted for each candidate structures associated with the molecular ion *m/z* 155.0816 including 3-(5-oxo-4,5-dihydro-*1H*-pyrrol-2-yl)propenamide (**1**), 3-(1-methyl-*1H*-imidazol-2-yl)propanoic acid (**2**), 3-(1-methyl-*1H*-pyrazol-5-yl)propanoic acid (**3**), 3-(1-methyl-*1H*-imidazol-4-yl)propanoic acid (**4**), 3-(1-methyl-*1H*-imidazol-5-yl)propanoic acid (**5**) and 4-(*1H*-pyrazol-1-yl)butanoic acid (**6**) using ChemDraw and NMRium (Patiny et al., 2024) (Figure 1). Candidate structures were downgraded in priority if there was no ^{1}H NMR signal within ± 0.15 ppm of predicted signals in blue crab urine or urine extract ^{1}H NMR spectra. Using 2D NMR (COSY, HSQC, HMBC) of blue crab urine extract, candidate structure coupling (^{1}H -^{1}H, ^{1}H -^{13}C, and 2-to-3 bond ^{1}H -^{13}C) assignments were attempted. However, this was not feasible for complete structural assignment due to a considerable signal overlap in the chemically complex sample.

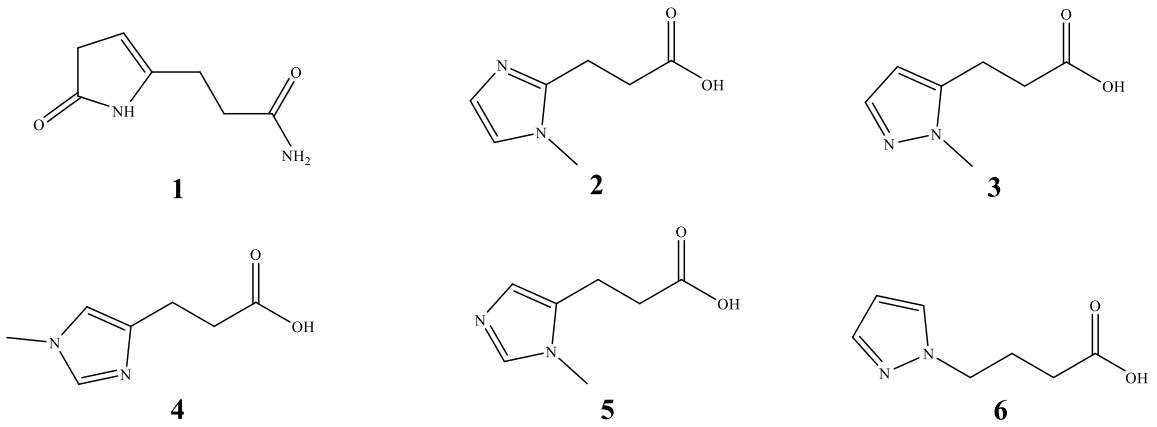

Figure 1 Molecular structures of candidate compounds for the metabolite in blue crab urine with $[M+H]^+$ *m/z* 155.0816: 3-(5-oxo-4,5-dihydro-*1H*-pyrrol-2-yl)propenamide (1), 3-(1-methyl-*1H*-imidazol-2-yl)propanoic acid (2), 3-(1-methyl-*1H*-pyrazol-5-yl)propanoic acid (3), 3-(1-methyl-*1H*-imidazol-4-yl)propanoic acid (4), 3-(1-methyl-*1H*-imidazol-5-yl)propanoic acid (5) and 4-(*1H*-pyrazol-1-yl)butanoic acid (6)

The approximate concentration of the metabolite with $[M+H]^+$ *m/z* 155.0816 was assessed using MS by comparing the feature's molecular ion peak area to the peak area of serially diluted standards using methods described in section 2.6 below. In order to exclude from consideration compounds whose commercial standards did not match UPLC retention time data, individual aliquots of a blue crab urine sample (BCO7) were each spiked with a single chemical standard or multiple standards in combination, at concentration(s) similar to that of the metabolite's expected concentration in blue crab urine. Spiked urine samples were analyzed UPLC-MS conducted with A Vanquish HPLC coupled to an Orbitrap ID-X Tribrid mass spectrometer. Each sample was injected in 1 µL volumes using an ACQUITY UPLC BEH Amide column (2.1 X 150 mm, 1.7 µm particle size, Waters Corporation). Metabolites were eluted at 40 µL/min using 4:1 water/acetonitrile with 10 mM ammonium formate and 0.1% formic acid (mobile phase A), and acetonitrile with 0.1% formic acid (mobile phase B) in the following gradient: 0 min 5% A; 0.5 min 5% A; 8 min 60% A; 9.4

min 60% A; 9.5 min 5% A; 12 min 5% A (Cepeda, 2023). Orbitrap ID-X Tribrid Mass Spectrometer heated electrospray ionization (HESI) settings were the following: positive ionization mode, spray voltage of 2.3 KV, sweep gas flows of 40, 8 and 1 L/hr, with a vaporizer temperature of 257 °C. Data were acquired for ions with *m/z* 40-178.6 at a resolution of 60,000. Targeted tandem mass spectral data was acquired for *m/z* 155.0816 in the ion trap with higher collision energy collisional dissociation (80 eV). Molecular ion retention times and peak overlap were used to assess chemical standards coeluting with the feature of interest.

2.6 MS sample preparation and analysis for metabolite quantification

Metabolite concentrations in blue crab urine were determined by comparing molecular ion peak areas (*m/z* 155.0816) from MS spectra to a calibration curve generated using commercial standards of candidate metabolites. MS and MS^2 data for standards as well as for the blue crab urine sample containing the highest concentration of this metabolite (BCO7) were collected using the methods described in section 2.5. The chemical standards were purchased from Sigma Aldrich Inc. (for **2**), Enamine US Inc. (for **4**), and BLD Pharmatech Co. Ltd. (for **5**). For each standard, a serial dilution with a 1:10 dilution factor was prepared using MeOH for dilution resulting in final concentrations of 10 nM to 1.0 µM, 11 nM to 1.1 µM, and 10 µM to 1.0 µM for **2**, **4**, and **5**, respectively.

The *m/z* 155.0816 molecular ion peak area for each injected sample was integrated using Freestyle software. Peak areas and concentration were log-transformed and fitted via linear regression in GraphPad Prizm 10. The resulting linear function was used to interpolate metabolite concentrations in a 9:1 (v/v) MeOH and BCO7 urine sample. The

calculated concentration in the diluted sample was multiplied by 10 to determine the concentration in the undiluted sample. Metabolite concentrations in other samples were calculated relative to the BCO7 sample using molecular ion intensity for MS data initially acquired by Marisa Cepeda described in Section 2.1 (Cepeda, 2023). Concentration mean and standard deviation were calculated for each calibration curve, ensuring accurate quantification of the metabolite across all samples.

2.7 Oyster shell strengthening assay to assess candidate chemical cues

Oyster (*Crassostrea virginica*) shell strengthening assays were conducted by collaborators at Dauphin Island Sea Lab using blue crab urine mixtures using methods previously described (Roney et al., 2023; Cepeda, 2023). Seawater used in bioassays was collected from the Gulf of Mexico, filtered to 200 µM, and settled for three days before use. Oyster larvae were sourced from the Auburn University Shellfish Laboratory and settled onto 4.5 cm X 4.5 cm marble tiles. Post-settlement spat were held for five days in 1250 L mesocosms with a constant flow of filtered (200 µM) before bioassays. After five days, tiles with eight or more spat were affixed in pairs, and four tile pairs were suspended in 2 L aquaria using a polyethylene fishing line. Aquaria were filled with 2 L of filtered (200 µM) and settled seawater. Air stones were placed in each aquarium to provide constant oxygenation and water flow. Spat were fed with 0.5 ml of Reed Mariculture Shellfish Diet 1800 twice daily.

Oyster spat were exposed to chemical cues known to induce oyster shell strengthening (homarine and trigonelline; Roney et al. 2023), along with the newly identified cues from this investigation. Treatment groups incorporated metabolites

individually and in combinations as described in Table 2. Prescribing cues individually and in combined treatment groups allowed us to assess if a combination of cues induced shell strengthen differently than individual cues. For treatments combining candidate compounds associated with the same molecular feature (*m/z* 155.0816), each compound was included at the same concentration adding up to the total concentration used for those metabolites tested individually (8.6 nM). Additional treatments included predator water as positive control (0.5 L of water from a 238 L tank containing six blue crabs with 1.5 L of seawater) and negative control using only seawater (Table 1). Each of the thirteen treatments was conducted with eight replicate aquaria each containing numerous oyster spat. Twice weekly, aquaria were cleaned, aquarium water was changed, and treatments were reintroduced.

After eight weeks, tiles containing oyster spat were collected from each aquarium and the length of each spat was measured using calipers. The crushing force of each spat was measured using a Kistler 5811A handheld charge amplifier coupled to a 9307-force sensor. Crushing force and length measurements were taken for all surviving spat in each replicate, up to 32 spat per replicate aquarium. The standardized crushing force was calculated for each spat defined by the force (N) required to crush the spat per unit length (mm).

Two statistical approaches were used to evaluate the bioassay data: 1) a Kruskal-Wallis test with a Dunn's multiple comparison test, and 2) an a priori general linear mixed model (GLMM) with a post hoc pairwise comparison. Combining these statistical approaches allowed the data to be evaluated from both parametric and non-parametric perspectives, ensuring the results were not reliant on one distributional assumption.

The nonparametric Kruskal-Wallis test and Dunn's multiple comparison test were conducted using Prism GraphPad. The Dunn's multiple comparison test compared the mean ranks of each treatment to the mean rank of the negative control (SW) and reported the multiplicity adjusted p value. Prior to nonparametric testing the ROUT (1%) function was used to remove outliers resulting from operator error or environmental factors affecting individual data points.

The GLMM, using R, was applied to account for the nested experimental design and hierarchical data structure with tiles nested in tile pairs and nested in jars. Dr. Benjamin Belgrad conducted GLMM statistical tests and post hoc pairwise comparisons. Prior to statistical analysis, jars with ten spat or fewer were removed, including two positive control (predator water [PW]) replicates, one from the treatment with **4**, one from **4** + **5** + H + T, and two from **2** + **4** + **5**. The GLMM was run using the lme4 package with a gamma distribution and included a fixed effect for treatment, a 13-category one factorial variable. Random effects accounted for the nested experimental design with tiles nested in tile pairs nested in aquaria. The model compared each treatment to the seawater control. Results were assessed using the Anova() function from the car package, which provided a chi-squared value, p-value, and the overall treatment effect compared to the negative control (SW). In addition to the a priori GLMM, post hoc pairwise comparisons were performed using the GLHT() function from the multcomp package with Tukey constraints.

Table 1: Oyster shell strengthening assay treatments, using individual and combinations of commercial standards including 3-(1-methyl-*1H*-imidazol-2-yl) propanoic acid (2), 3-(1-methyl-*1H*-imidazol-4-yl) propanoic acid (4), and 3-(1-methyl-*1H*-imidazol-5-yl) propanoic acid (5), as well as homarine (H) and trigonelline (T).

Abbreviation	Treatment
SW	Seawater
PW	Seawater (1.5 L) and blue crab tank water (0.5 L)
2	**2** (8.6 nM)
4	**4** (8.6 nM)
5	**5** (8.6 nM)
4 + 5	**4** (4.3 nM), **5** (4.3 nM)
2 + 4 + 5	**2** (2.9 nM), **4** (2.9 nM), **5** (2.9 nM)
H + T	Homarine (6.9 nM), and trigonelline (18 nM)
2 + H + T	**2** (8.6 nM), homarine (6.9 nM) and trigonelline (18 nM),
4 + H + T	**4** (8.6 nM), homarine (6.9 nM), and trigonelline (18 nM)
5 + H + T	**5** (8.6 nM), homarine (6.9 nM), and trigonelline (18 nM)
4 + 5 + H + T	**4** (4.3 nM), **5** (4.3 nM), homarine (6.9 nM) and trigonelline (18 nM)
2 + 4 + 5 + H + T	**2** (2.9 nM), **4** (2.9 nM), **5** (2.9 nM), homarine (6.9 nM) and trigonelline (18 nM)

CHAPTER 3. RESULTS

3.1 Selection of molecular features correlated with shell strengthening

The work by Marisa Cepeda identified mass spectral features important to the shell-strengthening response, and this investigation identified the molecular structures of the corresponding molecular features. To do this, Cepeda (2023) used a partial least square regression (PLS-R) model with genetic algorithm variable selection to identify specific metabolites from blue crab urine that induce oyster shell strengthening. Models were applied to blue crab urine mass spectral (MS) datasets and oyster shell strengthening bioassay data, seeking a correlation between concentrations of urinary metabolites and urine potency in affecting oyster shell strength (Cepeda 2023, Section 2.2). This method allowed for high-accuracy profiling of molecules within urine samples that contribute the most to oyster shell strengthening. Variable importance of parameter (VIP) scores generated for each molecular feature indicate the features contribution to the model (Cepeda 2023, Section 2.3). The top ten features were selected for further annotation and structural identification (Table 2). The accurate mass of these molecules was used to calculate molecular formulae and for targeted MS/MS (MS^2) analysis (Cepeda 2023, Section 2.2).

Table 2: The ten molecular features in blue crab urine most correlated with oyster shell strengthening, derived from UPLC-MS metabolomics data in positive ionization mode (taken from Cepeda 2023). Chromatographic separation was conducted using a HILIC ACQUITY UPLC BEH Amide column (2.1 × 150 mm, 1.7 µm particle size, Waters Corporation) 1 µL injection volumes. Variable importance of parameter (VIP) scores were calculated from PLS-R models after the list of molecular features was refined with genetic algorithm variable selection. Higher VIP scores indicate the relative importance of each molecular feature to the shell-strengthening model. ACQUITY UPLC BEH Amide column (2.1 × 150 mm, 1.7 µm particle size, Waters Corporation)

Molecular Feature ($[M+H]^+$ *m/z)*	Retention Time (min)	Molecular Formula of molecular ion $[M+H]^+$	VIP Score
155.0816	4.97	$C_7H_{10}N_2O_2$	3.3
392.1602	1.55	$C_{22}H_{21}N_3O_4$	2.3
230.1499	7.09	$C_{10}H_{19}N_3O_3$	2.0
214.0686	1.40	$C_7H_{13}NO_5$	1.8
309.1379	6.21	$C_{14}H_{20}N_4O_2S$	1.8
250.0379	1.46	$C_8H_{11}NO_6S$	1.6
276.1264	4.40	$C_{12}H_{21}NO_4S$	1.5
269.1384	1.02	$C_{14}H_{20}O_5$	1.5
243.1340	4.81	$C_{11}H_{18}N_2O_4$	1.5
234.1340	5.16	$C_{10}H_{19}NO_5$	1.4

3.2 Evaluation of SPE-extracted urine ^{1}H NMR spectra: Signal-to-Noise Enhancement and Feasibility for Structural Elucidation

When concentrated by reversed-phase solid-phase extraction (SPE), the signal-to-noise ratio of the extracted blue crab urine (sample BCO3) ^{1}H NMR spectrum was enhanced by a factor of three relative to BCO3 urine while preserving critical ^{1}H signals for structural elucidation (Figure 2).

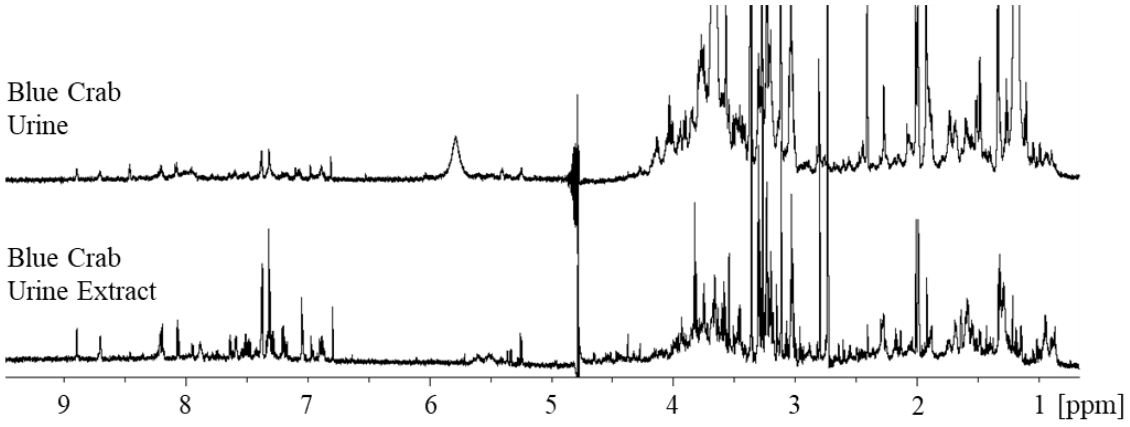

Figure 2: ^{1}H NMR spectra of a blue crab urine (sample BCO3) before (top) and after (bottom) concentration by solid-phase extraction (SPE) (800 MHz, in buffered D2O with water suppression).

Due to the inherent chemical complexity of blue crab urine, substantial ^{1}H NMR signal overlap was observed, precluding resolution of peak shape and accurate *J*-coupling measurements for individual signals. Consequently, the ^{1}H NMR spectrum of the BCO3 urine extract was primarily employed to refine the list of candidate structures towards metabolite identification, based on the presence or absence of signals in the less-crowded downfield region of the spectrum, within a tolerance of $\pm\ \delta\ 0.15$, corresponding to chemical shifts predicted ^{1}H NMR spectra or observed in experimental ^{1}H spectra of reference standards.

3.3 Identification of Prioritized Metabolites

3.3.1 Generating candidate structures from MS and MS^2 data

The molecular formulae presented by Cepeda (2023) were used along with MS^2 spectral data to search publicly available MS databases and for *de novo* structure prediction. Candidate structures for five of the ten selected blue crab urine metabolites were compiled based on database hits from public databases (Table 3). Additionally, candidate structures for four molecular features were predicted using SIRIUS and CSI:FingerID (Table 4). They include molecules belonging to structural classes such as imidazoles, amides, and sulfated phenols. Candidates ranged from being likely chemical components of urine, such as derivatives of histidine, to ones that are unlikely to be components of urine with pyrimidinetyrione core with three carbonyl groups (Sui et al., 2021).

Table 3: LC-MS fragment ions for features important to the PLS-R metabolomics model of blue crab urine (Cepeda, 2023), detected using stepped higher-energy collisional dissociation (HCD) energies of 15, 30, and 45 eV, as well as collision-induced dissociation (CID) energy of 45 eV. Ions highlighted in bold correspond to matches with commercial standard or database spectra. The level of confidence for each spectral match was assigned a rating from 1 to 4, based on the following criteria: 1) match of accurate mass, molecular isotope peaks, retention time, and MS/MS spectrum with a standard; 2) match of accurate mass, molecular isotope peaks, and MS/MS spectrum consistent with literature data; p) Putative identification of compound class based on chromatographic elution window, accurate mass, and molecular isotope; or 4) no clear matches.

m/z	Molecular Formula of charged ion $[M+H]^+$	Compound Number	Candidate molecular structure	MS-MS Ionization Method	*m/z* of Fragment Ions Observed in MS/MS Experiments	Confidence Level	Match Details (Source)
155.0816	$C_7H_{10}N_2O_2$	1	3-(5-Oxo-4,5-dihydro-1H-pyrrol-2-yl)propanamide	HCD	133.11, **109.46**, 108.87, 98.16, 96.71, **95.06**, 94.36, 58.08	2	Consistent with spectra (NIST Spectra)
				CID	**138.01, 137.05, 136.13, 127.06, 114.08, 113.19, 112.19, 111.22, 109.01, 96.45, 95.01, 82.13, 81.02, 72.95, 72.13, 58.01**		
		2	3-(1-methyl-1*H*-imidazol-2-yl)propanoic acid	HCD	**133.11**, **109.46**, **108.87**, 98.16, 96.71, **95.06**, 94.36, **58.08**	1	Consistent with standard
				CID	138.01, **137.05**, 136.13, 127.06, 114.08, 113.19, 112.19, 111.22, **109.01**, 96.45, **95.01**, 82.13, **81.02**, 72.95, 72.13, 58.01,		
		4	3-(1-methyl-1*H*-imidazol-4-yl)propanoic acid	HCD	133.11, **109.46**, 108.87, 98.16, 96.71, **95.06**, 94.36, **58.08**	1	Consistent with standard (Enamine US Inc)
				CID	**138.01**, **137.05**, 136.13, 127.06, 114.08, 113.19, 112.19, 111.22, **109.01**, 96.45, **95.01**, 82.13, 81.02, 72.95, **72.13**, **58.01**,		
		5	3-(1-methyl-1*H*-imidazol-5-yl)propanoic acid	HCD	133.11, **109.47**, 108.88, 96.72, 98.17, **95.06**, **94.37**, **58.08**,	1	Consistent with standard (BLD Pharmatech Co.
				CID	138.01, **137.05**, 136.13, 127.06, **114.08**, 113.19, 112.19, 111.22, 109.01, **96.45**, **95.01**, 82.13, 81.02, 72.95, **72.13**, **58.01**,		
		6	4-(1*H*-pyrazol-1-yl)butanoic acid	HCD	133.11, **109.46**, **108.87**, 98.16, 96.71, 95.06, 94.36, 58.08	2	Consistent with spectra (PubChem)
				CID	138.01, **137.05**, 136.13, 127.06, 114.08, 113.19, 112.19, 111.22, **109.01**, 96.45, 95.01, 82.13, **81.02**, 72.95, 72.13, 58.01,		
392.1602	$C_{22}H_{21}N_3O_4$	7	Ethyl 4-[(E)-{[2,5-dimethyl-1-(3-nitrophenyl)-1H-pyrrol-3-yl]methylene}amino]benzoate	HCD	56.76, 58.56, 62.44, 64.75, 65.55, 67.92, 68.86, 78.20, 79.87, 85.03, 89.06, 97.80, 98.07, 99.14, 114.11, 118.06, 130.06, 130.95, 135.20, 145.11, 158.06, 160.08, 162.54, 164.24, 172.08, 189.10, 198.76, 199.09, 201.10, **202.08**, 202.09, **217.10**, 227.08, 245.09, 260.13, 337.30, 343.87	2	Consistent with spectra (ChemSpider)
				CID	106.29, 107.73, 108.10, 109.62, 110.34, 111.52, 115.15, 115.28, 115.76, 118.16, 122.55, 128.05, 130.07, 156.71, 157.68, 158.06, 160.08, 169.78, 171.00, 174.05, 179.77, 181.74, 184.71, 189.10, 199.09, **202.09**, **217.10**, 219.11, 222.82, **227.08**, 229.10, 235.11, 235.37, 245.09, 247.11, 253.57, 275.10, 275.12, 287.12, 290.65, 315.11, 319.14, 328.14, 329.13, 333.12, **344.14**, 344.89, **346.15**, 347.28, **356.14**, 357.12, **362.15**, **374.15**, 375.31, 382.60		
250.0379	$C_8H_{11}NO_6S$	18	4-[(1*R*)-2-Amino-1-hydroxyethyl]-2-hydroxyphenyl hydrogen sulfate	HCD	54.81, 70.62, 85.78, 89.69, 103.83, **109.41**, 124.47, 130.59, 148.42, **189.93**, 214.77, 225.29	2	Consistent with spectra (PubChem)
				CID	**109.09**, 125.17, 127.89, **138.10**, 142.02, 146.89, **150.09**, **151.00**, 162.04, 163.02, 164.01, **166.13**, **167.19**, 168.27, 170.08, **172.19**, **190.19**, **191.17**, 193.2, 194.44, **204.09**, **208.08**, **209.2**, 222.3, **232.08**, **233.04**		
269.1384	$C_{14}H_{20}O_5$	19	2,5,8,11,14-pentaoxabicyclo[13.4.0]nonadeca-1(19),15,17-triene	HCD	57.21, 57.66, 60.89, 63.93, 70.14, 77.48, 77.83, 109.36, 121.37, 134.89, 141.02, 173.45, 242.32, 245.29, 246.54	2	Consistent with spectra (ChemSpider)
				CID	80.90, 84.13, **95.03**, 99.03, **101.17**, **107.25**, **109.20**, **111.14**, **119.10**, 120.04, **123.09**, 124.06, **131.07**, **132.36**, 142.89, **147.16**, **149.02**, **151.14**, **163.05**, 167.99, 169.01, **173.16**, **177.10**, **179.07**, **181.08**, 187.08, 189.14, **191.21**, **193.14**, **195.11**, **195.42**, **205.19**, **207.09**, **209.23**, **211.05**, 211.84, **213.00**, 214.41, 215.17, 215.48, 216.09, **223.19**, **224.12**, **225.12**, **226.57**, **227.23**, 227.74, 228.25, 232.79, 233.16, 233.85, **237.19**, **241.17**, 248.49, **250.51**, **251.10**, **251.64**, **252.08**, **254.14**, **254.82**, **269.07**		
243.1340	$C_{11}H_{18}N_2O_4$	20	5-Ethyl-5-(4-hydroxy-2-pentanyl)-2,4,6(1H,3H,5H)-pyrimidinetrione	HCD	60.21, 60.99, 70.11, 84.61, 93.04, 96.15, 103.85, 111.88, 114.99, 120.86, 143.17, 145.31, 160.20, 73.45, 179.52, 190.04, 197.25, 214.84	2	Consistent with spectra (ChemSpider)
				CID	84.05, **85.02**, 103.11, **121.20**, **132.97**, **139.09**, **141.1**, **144.05**, 159.01, **163.12**, 167.11, **169.04**, **172.13**, 179.03, **183.30**, **184.02**, **185.01**, **189.14**, 196.97, 201.08, **202.07**, **203.18**, **208.02**, **212.02**, 213.94, 215.07, **225.10**, **226.12**, **228.09**, **242.01**		

Table 4: Candidate metabolites predicted using SIRIUS and CSI:FingerID for four molecular features important to the PLS-R metabolomics model of blue crab urine (Cepeda et al, 2023). An exact match in CSI:FingerID scores 0. The Tanimoto similarity score measures the ratio of shared features between molecules, with a score of 0.85 indicating that compounds have 85% similarity in biological activity to known compounds (Jasial et al., 2016).

m/z	Molecular Formula of Charged Ion $[M+H]^+$	Compound Number	Candidate Molecular Structure	CSI:FingerID Score	Tanimoto Similarity Score	Match Details (Source)
155.0816	$C_7H_{10}N_2O_2$	2	3-(1-methyl-*1H*-imidazol-2-yl)propanoic acid	-48.48	0.72	PubChem
		3	3-(1-methyl-*1H*-pyrazol-5-yl)propanoic acid	-46.09	0.72	PubChem
		4	3-(1-methyl-*1H*-imidazol-4-yl)propanoic acid	-44.29	0.77	KEGG Mine
		5	3-(1-methyl-*1H*-imidazol-5-yl)propanoic acid	-41.70	0.76	PubChem
		6	4-(*1H*-pyrazol-1-yl)butanoic acid	-55.21	0.66	PubChem
392.1602	$C_{22}H_{21}N_3O_4$	8	2-[4-(morpholine-4-carbonyl)-2-oxoquinolin-1-yl]-N-phenylacetamide	-85.14	0.75	COCONUT, Pubchem, SuperNatural
		9	N-butyl-2-[4-[2-(4-nitroanilino)-2-oxoethyl]phenyl]acetamide	-277.78	0.35	DSSTox, MeSH, PubChem
		10	3-(1,3-dioxoisoindol-2-yl)-N-[3-[(2-oxopyrrolidin-1-yl)methyl]phenyl]propanamide	-283.65	0.35	DSSTox, PubChem
		11	N-[2-[[4-[(4-methylbenzoyl)amino]benzoyl]amino]ethyl]furan-2-carboxamide	-285.87	0.30	PubChem
		12	N-(5-acetamido-2-methoxyphenyl)-1-benzyl-2-oxopyridine-3-carboxamide	-288.94	0.34	PubChem
230.1499	$C_{10}H_{19}N_3O_3$	13	3-acetamido-N-(3-acetamidopropyl)propanamide	-44.41	0.70	PubChem
		14	N-(2-acetamidoethyl)-N'-butylethanediamide	-83.99	0.66	PubChem
		15	3-amino-N-(3-oxo-3-((3-oxobutyl)amino)propyl)propanamide	-64.59	0.72	PubChem
		16	2,6-diacetamidohexanamide	-60.40	0.63	PubChem, KEGG Mine
		17	6-acetamido-N-(2-amino-2-oxoethyl)hexanamide	-86.50	0.66	PubChem

3.3.2 Structural analysis for metabolite with $[M+H]^+$ m/z 155.0816

Priority was given to exploring candidate structures associated with the feature with $[M+H]^+$ *m/z* 155.0816 as it exhibited the highest VIP score (3.3) indicating that it represented the metabolite within blue crab urine most important for oyster shell strengthening (Cepeda 2023). The molecular formula for this compound was $C_7H_{10}N_2O_2$ with four degrees of unsaturation. Based on mass spectral MS^2 database matches, Tanimoto similarity scores between 0.66 and 0.76, and CSI:FingerID scores between -55.21 and -41.70 the following, candidate compounds were associated with this feature: 3-(5-oxo-4,5-dihydro-*1H*-pyrrol-2-yl)propenamide (**1**), 3-(1-methyl-*1H*-imidazol-2-yl)propanoic acid

(**2**), 3-(1-methyl-*1H*-pyrazol-5-yl)propanoic acid (**3**), 3-(1-methyl-*1H*-imidazol-4-yl)propanoic acid (**4**), 3-(1-methyl-*1H*-imidazol-5-yl)propanoic acid (**5**) and 4-(*1H*-pyrazol-1-yl)butanoic acid (**6**) (Figure 1).

Among candidates for the molecular feature with *m/z* 155.0816, **4**, and **5** were the most likely as these molecules are modified histidine derivatives. With a methylated imidazole ring attached to a propanoic acid chain, these molecules are structurally similar to the amino acid histidine, frequently excreted in urine, at least in humans (Dunstan et al., 2017,). Candidates **4** and **5** are highly feasible as possible components of blue crab urine as they could be synthesized through the deamination and methylation of histidine through known biosynthetic pathways (Figure 1) (Stifel & Herman, 1971). The carboxylic acid group in **2**, **5**, and **6** would contribute positively to their water solubility, making their excretion via urine possible. Without a carboxylic acid group, **1** is less soluble in water than other candidates for this feature, making it less likely to be efficiently dissolved and excreted in urine than other candidates.

The MS^2 fragments observed for this unknown metabolite that matched data for fragments reported in databases or by comparison with authentic chemical standards are listed in Table 3. Candidate **1**, identified through database matching, was not predicted *in silico* (Table 4). Although **2**, **4**, **5**, and **6** were predicted by *in silico* MS fragmentation as well as through database matching, **3** was only predicted *in silico* and could only be evaluated based on its CSI:FingerID score. Positively charged daughter ions with *m/z* 137.05, 109.01, and 95.01 each had a CSI:FingerID score of 100%, corresponding to a respective loss of OH, CH_2O_2, and $C_2H_4O_2$, consistent with **3** (Table 4). Each of these candidate molecules contained a five-member ring, all but one of which were composed of

$C_3N_2H_3$ consistent with the fragment at *m/z* 95.06 with a calculated molecular formula $C_5H_6N_2$ corresponding to the methylated ring structure. Furthermore, all candidates except **1** had an ethyl (**2-5**) (or propyl (**6**)) linker terminating in a carboxyl group consistent with the positive daughter ion *m/z* 109.076 with a molecular formula of $C_6H_8N_2$ indicative of the loss of CHO_2. Candidates **2-6** differed in the location and methylation of the aromatic nitrogen. The similarities of these generated *in silico* and through database matching indicated the unknown compound was likely one of these candidates with a carboxyl group and an aromatic ring structure with a formula of $C_3H_2N_2$.

Candidates **1-6** were examined further by comparing their predicted ^{1}H NMR spectra to ^{1}H NMR spectra of blue crab urine (sample BCO3) (Figure 3). Due to the chemical complexity of blue crab urine, overlapping signals permeated the δ 0.7-4.5 spectral region of ^{1}H NMR spectrum of urine extract, making only spectral regions downfield of δ 4.5 useful for comparative analysis (Figure 2). Structure **1** was eliminated as there were no signals in blue crab urine extract spectrum at δ 5.00 $\pm$ 0.15 for the proton attached to ^{3}C predicted with nmrdb (Banfi & Patiny, 2008; Andrés et al, 2011; Aires-de-Sousa et al, 2022).

Chemical standards purchased for **2-6** were assessed based on their ^{1}H NMR spectra, MS^2, and UPLC-MS chromatographic elution time. The ^{1}H NMR spectrum of each standard (Figure 3) was compared to blue crab urine extract ^{1}H NMR spectra (Figure 2). Candidates **3** and **6** were considered incompatible with the urinary metabolite based on ^{1}H NMR signals at δ 6.30 and δ 6.18 observed in ^{1}H NMR spectra acquired for each respective standard (Figure 3), which were absent in blue crab urine and urine extract spectra (Figure 2).

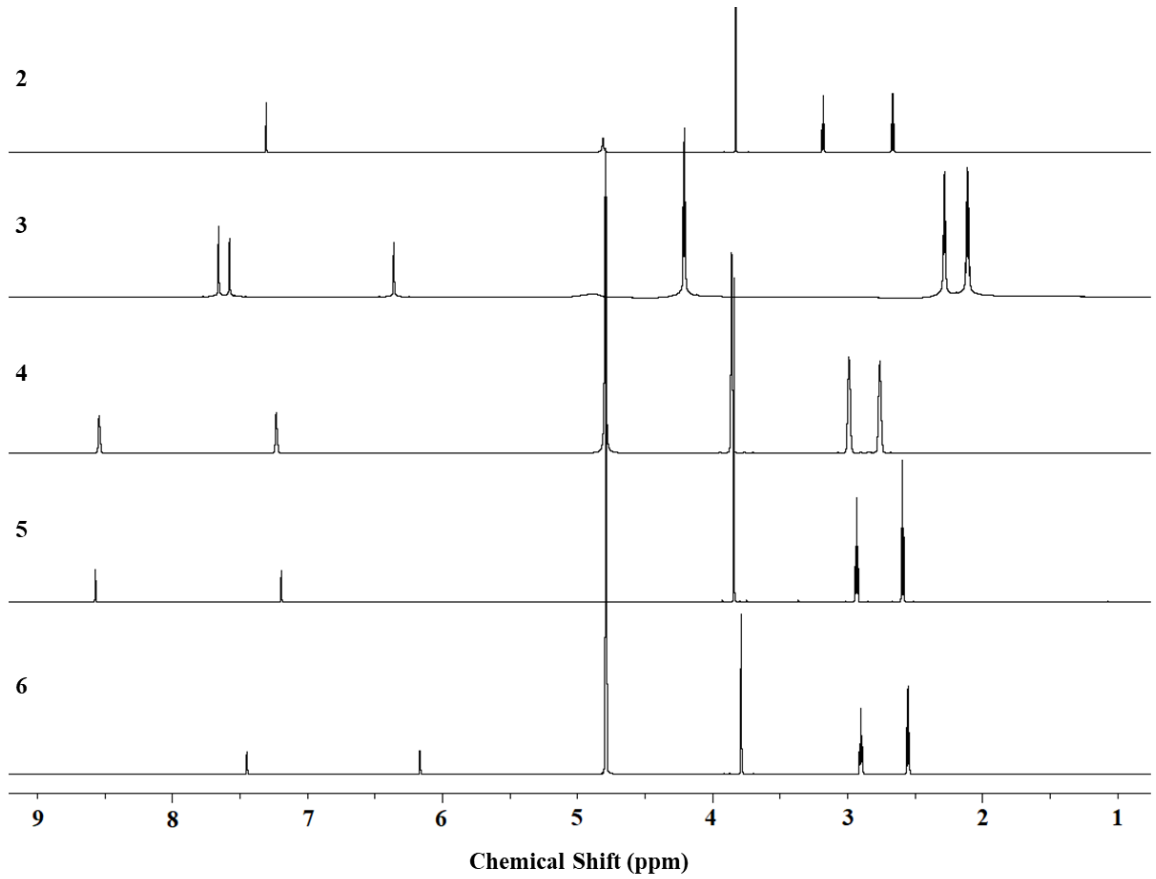

Figure 3: ^{1}H NMR spectra commercial standards of 3-(1-methyl-*1H*-imidazol-2-yl)propanoic acid (2), 3-(1-methyl-*1H*-pyrazol-5-yl)propanoic acid (3), 3-(1-methyl-*1H*-imidazol-4-yl)propanoic acid (4), 3-(1-methyl-*1H*-imidazol-5-yl)propanoic acid (5) and 4-(*1H*-pyrazol-1-yl)butanoic acid (6) (800 MHz, in buffered D_2O with water suppression). Numbers to the left of each ^{1}H NMR spectra indicate the compound associated with that spectrum.

Candidates **2, 4,** and **5** were further refined by comparing reversed-phase UPLC-MS chromatographic properties of authentic standards to that of the metabolite of interest with $[M+H]^+$ *m/z* 155.0816, whose retention time on a BEH amide column was 4.96 min (Figure 4). A second extracted ion with $[M+H]^+$ *m/z* 155.0816 was observed in blue crab urine with a retention time of 7.25 min. However, this ion was not identified as important to shell strengthening models (Cepeda 2023, Figure 4). Retention times were 5.39 (**2**), 5.03

(**4**), and 5.23 (**5**) min when analyzed individually and 5.43 (**2**), 5.06 (**4**), and 5.25 (**5**) min when spiked into blue crab urine (sample BCO7) (Figure 4).

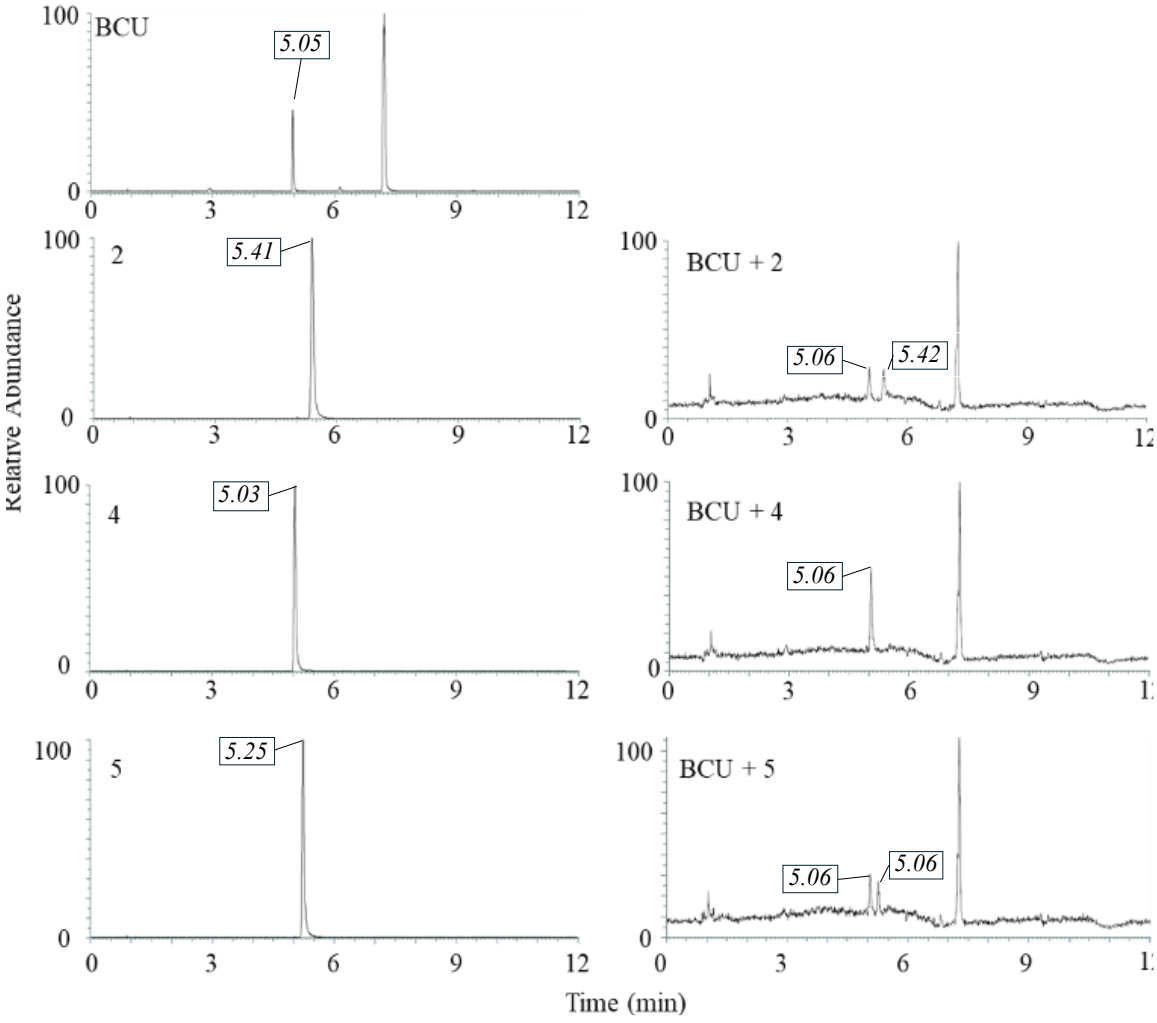

Figure 4: Extracted ion chromatogram (EIC) on a BEH amide column for molecular ion [M+H]+ *m/z* 155.0816 from blue crab urine (BCU) and commercial standards for candidates 3-(1-methyl-*1H*-imidazol-2-yl)propanoic acid (2), 3-(1-methyl-*1H*-imidazol-4-yl)propanoic acid (4), and 3-(1-methyl-*1H*-imidazol-5-yl)propanoic acid (5). Labels at the top left of each EIC indicate the solution: blue crab urine (BCU), 2, 4, and 5; and spiked combinations (BCU + 2, 4, or 5; BCU + 2 + 4 + 5). Retention times (RT) in minutes are listed in italics the ion peaks corresponding the ion of interest ($[M+H]^+$ *m/z* 155.0816) or chemical standards 2, 4 and 5.

The identification of **4** as the metabolite of greatest interest in blue crab urine is strongly supported by the observed increase in peak area in urine spiked with an authentic

standard of **4** (Figure 4). Initially, the unknown feature in the blue crab urine displayed a peak at 5.05 minutes with an area of 2.21 x 10^5. When a commercially acquired **4** was individually spiked into blue crab urine, this peak, at approximately the same retention time (5.06 min), showed a substantial increase to 4.9 x 10^5. This doubling of peak area without the addition of an additional peak suggested that the standard co-eluted precisely with the unknown metabolite. Importantly, **4** alone, when analyzed as an authentic standard, exhibited a peak area of 2.70 x 10^5 at a nearly identical retention time (5.05 min), further validating that the increased peak area in the spiked sample can be attributed directly to the presence of **4**.

The assignment of the blue crab urine metabolite as **4** was confirmed by the lack of peak increase when authentic standards of **2** and **5** were each spiked into blue crab urine (Figure 4). In those cases, the peak area and retention time of the unknown feature in the urine remained relatively unchanged, and the two peaks (standard and urine metabolite) appeared side-by-side, ruling out the possibility that either **2** or **5** corresponds to the metabolite of interest. This result provided robust evidence that **4** is the metabolite of interest in blue crab urine responsible for the most significant role in statistical models assessing effects on oyster shell strength (Cepeda, 2023). Once **4** was identified, it was incorporated in a bioassay trial, along with **2** and **5**, to assess each compound's impact on oyster shell strengthening.

*3.3.3 Natural concentrations of 3-(1-methyl-1H-imidazol-4-yl)propanoic acid (**4**), in blue crab urine*

The concentration of 3-(1-methyl-*1H*-imidazol-4-yl)propanoic acid (**4**) was quantified in blue crab urine using UPLC-MS a calibration curve for the authentic standard of **4** (Figure 5). The limit of detection (LOD) was 0.07 nM, corresponding to the minimum concentration necessary for peak heights above the peak detection signal-to-noise (S/N) threshold of 1.5. The concentration of **4** in blue crab urine samples exhibited a substantial range from below 1 nM to 1.8 µM (Table 5). This variability in concentration highlights the metabolic diversity within individual blue crabs or differences in physiological states, with some samples presenting trace levels near 0.04 µM, while others reached significantly higher concentrations up to 1.8 µM. Multiple pooled urine samples from blue crabs fed oysters had concentrations at or above 0.3 µM which was observed for only one urine sample from blue crabs fed mud crabs, but the average concentration of **4** did not differ between each diet ($p = 0.67$; unpaired t test). As each urine sample was composed of the urine of multiple blue crabs, with each mixture using different individual crabs, the exact range of urinary concentrations from these blue crabs was not quantifiable. However, the observed variation of the chemical composition of urine for this compound was relatively high, with standard deviations of 0.49 µM among blue crabs fed oysters and 0.14 µM among blue crabs fed mud crabs (Table 5).

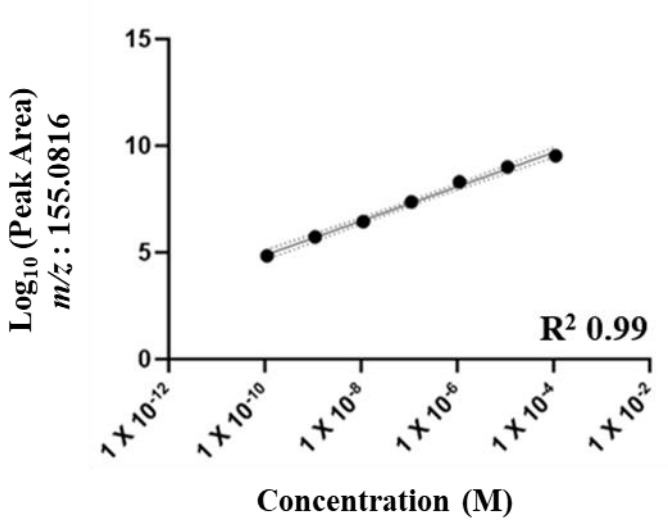

Figure 5: UPLC-MS calibration curve for quantification of 3-(1-methyl-1*H*-imidazol-4-yl)propanoic acid (4) in blue crab urine. Calibration coefficient (R^2) for the calibration curves indicate strong linearity across 6 orders of magnitude, from low nanomolar to high micromolar.

Table 5: Concentrations of 3-(1-methyl-*1H*-imidazol-4-yl)propanoic acid (4) in blue crab urine from blue crabs-fed oysters (BCO) and blue crabs-fed mud crabs (BCM), derived from UPLC-MS calibration curve with a commercial standard. The UPLC-MS calibration curve was used to calculate the concentration of 4 in blue crab urine sample BCO7, and then related to all other urine samples by comparison of the relative intensity of their molecular ion peaks from prior analyses (Cepeda, 2023). All concentrations, means, and standard deviations are listed µM. Samples for which the molecular ion peak height (at *m/z* 155.0816) was below the UPLC-MS signal-to-noise detection threshold (1.5) of approximately 0.07 nM are listed as zero.

Sample ID:	Concentration (µM)
BCO1	0.00
BCO2	0.35
BCO3	0.40
BCO4	0.16
BCO5	0.00
BCO6	0.00
BCO7	1.80
BCO8	0.09
BCO9	0.15
BCO10	0.15
BCO11	0.28
BCO12	0.00
$\bar{x}$ =	0.28 ∓ 0.49

Sample ID:	Concentration (µM)
BCM1	0.43
BCM2	0.26
BCM3	0.20
BCM4	0.11
BCM5	0.00
BCM6	0.03
BCM7	0.00
BCM8	0.22
BCM9	0.26
BCM10	0.00
BCM11	0.00
BCM12	0.00
$\bar{x}$ =	0.12 ∓ 0.14

3.3.4 Bioassay results for candidates of metabolite with $[M+H]^+$ m/z 155.0816

Oyster spat were exposed to **2**, **4**, and **5**, alone and in combination with each other and with homarine and trigonelline, at approximated environmental concentrations, taking into account their predicted concentrations in blue crab urine as well as the large expected dilution of urine in seawater.

The initial QQ plot generated in Prism Graph Pad distribution of the oyster shell strength data was ambiguous, with neither normal or lognormal QQ plots fitting the data, indicating that the data were not appropriate for parametric statistical tests., statistical outliers were removed from each treatment group using ROUT (Q = 1%), and normal and lognormal QQ plots were used to assess the dataset distrubution (Figure 7). The data was also assessed after replica aquaria with 10 surviving spat or were removed and significant differences were assessed with an a general lineraized mixed model (Figure 8).

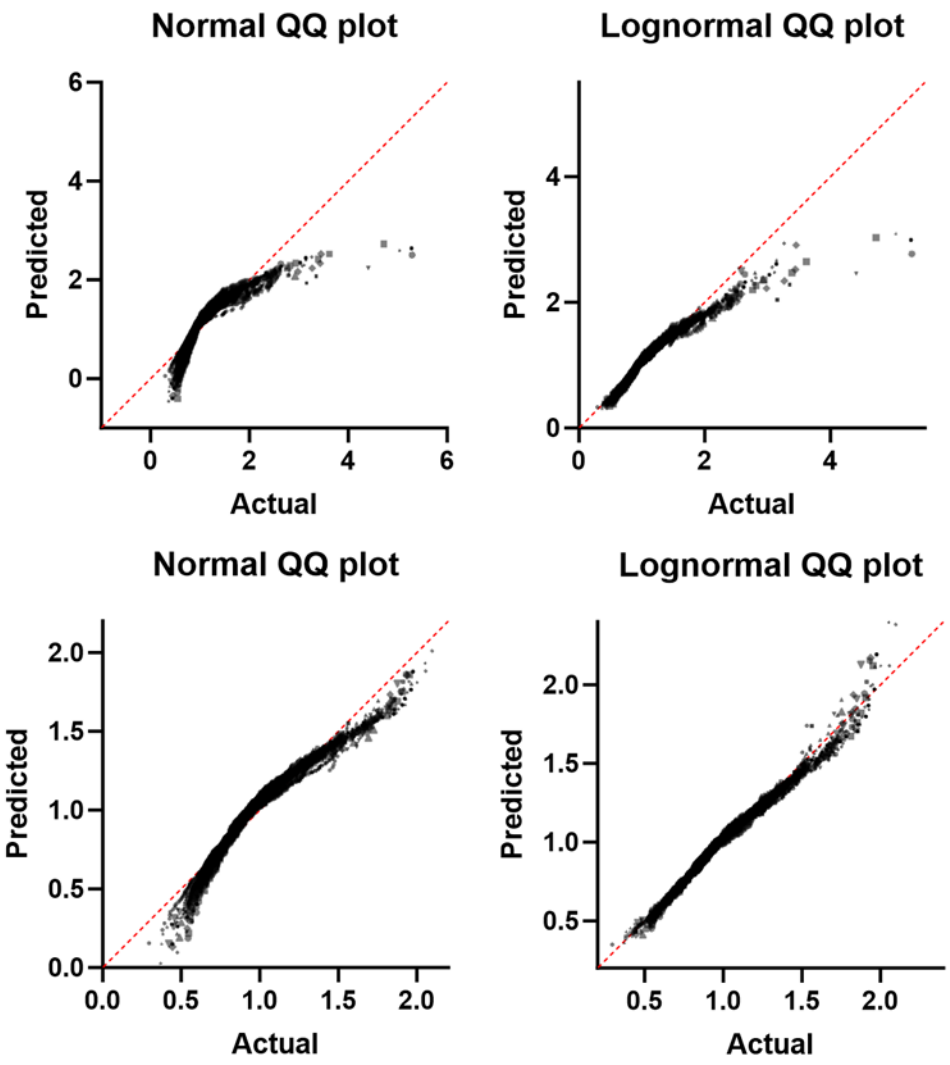

Figure 6: Normal and lognormal QQ plots before (top) and after (bottom) removing outlying crushing force data from each bioassay treatment with ROUT (Q = 1%).

3.3.4.1 Kruskal-Wallis and Dunns Multiple Comparison Statistical Analysis

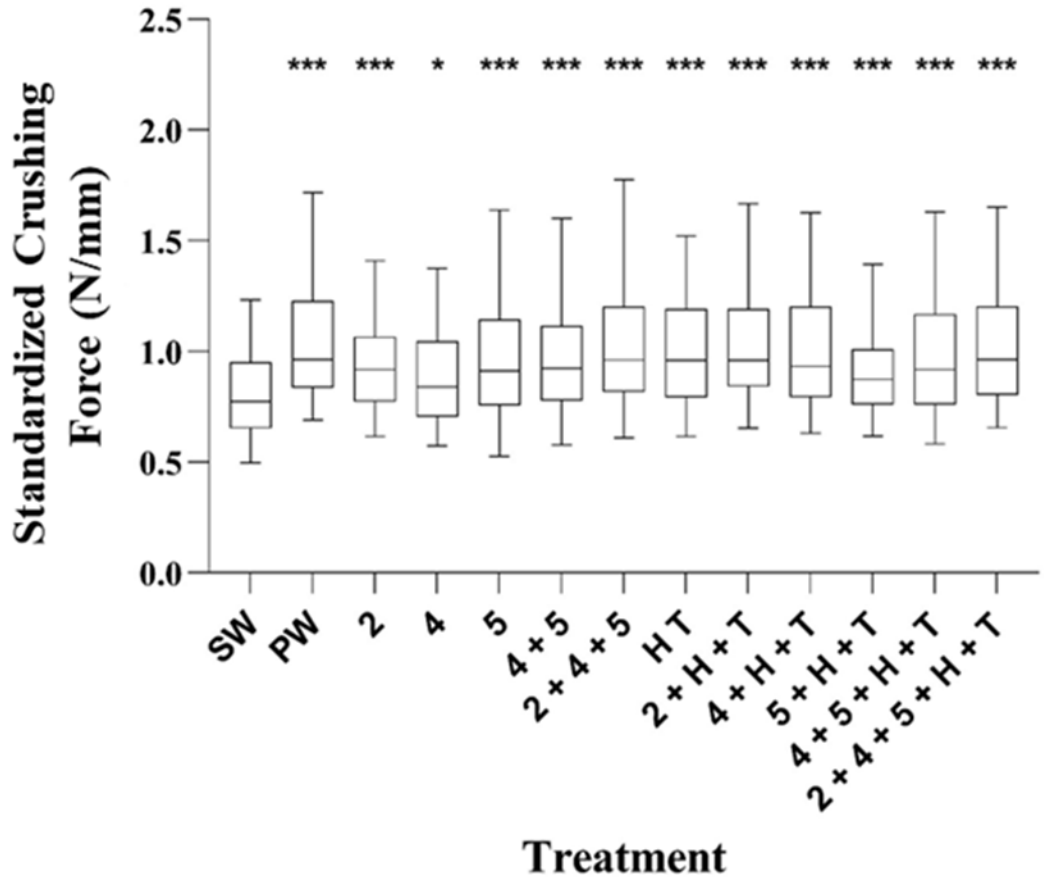

Figure 7: Oyster shell strengthening bioassay data using commercial standards for blue crab urine candidate metabolites. Asterisks indicate significant differences in each treatment compared with the negative (seawater) control (SW) at the 5% confidence level. Note: *** = p < 0.0001; * = p = 0.026. Treatment groups are seawater (SW); predator water (PW); 2 (8.6 nM) (2); 4 (8.6 nM) (4); 5 (8.6 nM) (5); 4 (4.3 nM), 5 (4.3 nM) (4 + 5); combination of 2 (2.9 nM), 4 (2.9 nM), 5 (2.9 nM) (2 + 4 + 5); combined homarine (6.9 nM) and trigonelline (18 nM) (H + T); 2 (8.6 nM), homarine (6.9 nM) and trigonelline (18 nM) (2 + H + T); 4 (8.6 nM), homarine (6.9 nM), and trigonelline (18 nM) (4 + H + T); 5 (8.6 nM), homarine (6.9 nM), and trigonelline (18 nM) (5 + H + T); 4 (4.3 nM), 5 (4.3 nM), homarine (6.9 nM) and trigonelline (18 nM) (4 + 5 + H + T); and a combination of 2 (2.9 nM), 4 (2.9 nM), 5 (2.9 nM), homarine (6.9 nM) and trigonelline (18 nM) (2 + 4 + 5 + H + T). Listed concentrations are the final concentration of each compound in bioassay aquaria, administered weekly for eight weeks.

After removing outliers with ROUT (1%) from each treatment, the bioassay data fit a lognormal distribution. When a Dunn's multiple comparison test was applied to the

data, a statistically significant difference was observed between all treatments and the seawater-only negative control, each with an adjusted p-value <0.0001, except for **4** whose p-value relative to the negative control was 0.026 (Figure 7). As such, all of the compounds tested induced oyster shell strengthening relative to seawater alone, including **4**, already identified as the metabolite most important to the oyster shell strengthening. The effect sizes, indicated by the boxplots, showed consistent and elevated median crushing force values across treatments compared to the negative control, with similar variability across groups, implying that individual metabolites and combinations of metabolites influence shell strength in a relatively consistent manner.

In this experiment, the positive control (conditioned water from blue crabs held in aquaria, also known as predator water), had a significantly positive shell induction effect compared to the uninduced control (SW) (Cepeda, 2023; Roney et al, 2023). In summary, all treatments, including **2**, induced shell strengthening, each of which was significantly different than the negative control group (SW) (Figure 7).

3.3.4.2 General Linear Mixed Model Statistical Analysis

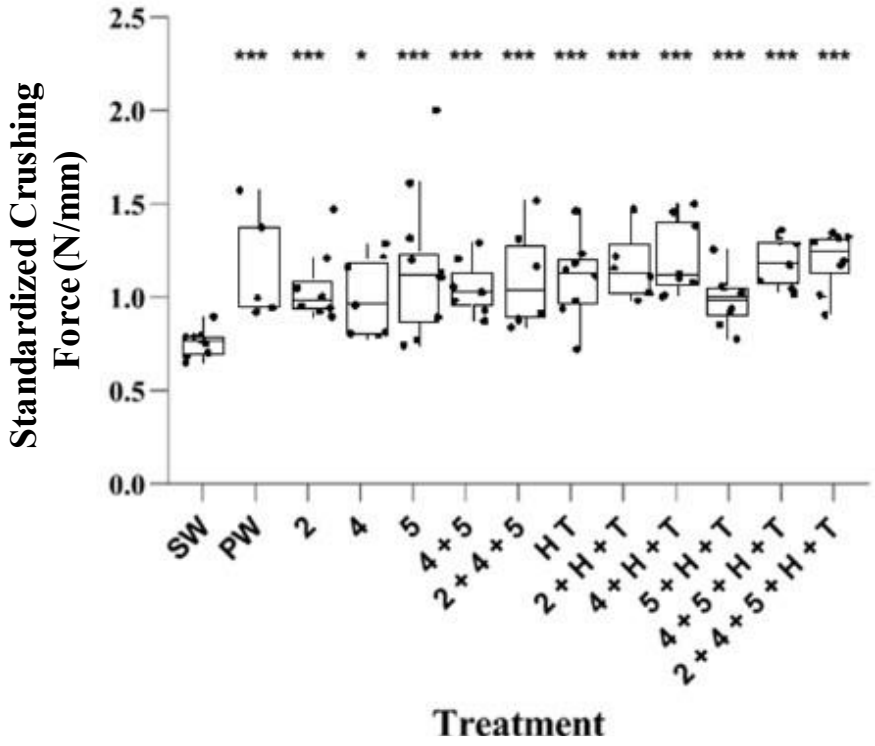

Figure 8: Oyster shell strengthening bioassay data analyzed by a general linear mixed model (GLMM) after removal of replicates with inadequate numbers of oyster spat. Note: * indicate significance at the 5% confidence level ($p \leq 0.05$) compared to seawater (SW); * indicates significance at the 10% confidence level ($p \leq 0.10$) compared to seawater (SW). Treatment groups are seawater (SW); predator water (PW); 2 (8.6 nM) (2); 4 (8.6 nM) (4); 5 (8.6 nM) (5); 4 (4.3 nM), 5 (4.3 nM) (4 + 5); combination of 2 (2.9 nM), 4 (2.9 nM), 5 (2.9 nM) (2 + 4 + 5); combined homarine (6.9 nM) and trigonelline (18 nM) (H + T); 2 (8.6 nM), homarine (6.9 nM) and trigonelline (18 nM) (2 + H + T); 4 (8.6 nM), homarine (6.9 nM), and trigonelline (18 nM) (4 + H + T); 5 (8.6 nM), homarine (6.9 nM), and trigonelline (18 nM) (5 + H + T); 4 (4.3 nM), 5 (4.3 nM), homarine (6.9 nM) and trigonelline (18 nM) (4 + 5 + H + T); and a combination of 2 (2.9 nM), 4 (2.9 nM), 5 (2.9 nM), homarine (6.9 nM) and trigonelline (18 nM) (2 + 4 + 5 + H + T). Listed concentrations are the final concentration of each compound in bioassay aquaria, administered weekly for eight weeks.**

After removing replicates with 10 or fewer surviving spat, the oyster shell strenghtening data fit a normal distribution. A general linearized mixed model (GLMM) with a gamma distribution and a fixed effect for treatment showed a statistically significant

difference between all treatments compared to the seawater control group, each with a p-value < 0.05, except for **4** which trended towards being significantly different from the negative control with a p-value of 0.062 (Figure 8). The overall treatment effect was significantly different compared to the negative control (SW) with a chi-squared value of 23, 12 degrees of freedom and p-value < 0.025. In addition to a priori GLMM results, a post hoc pairwise comparison using the GLHT() function from the multcomp package with Tukey constraints did not show statistical differences between any treatment groups other than the negative seawater control.

These results from the GLMM were congruent with those from the non-parametric Dunn's multiple comparison test, showing that all treatments induced oyster shell strengthening relative to the seawater control, including **4**, identified as the metabolite most important to the oyster shell strengthening models (Cepeda, 2023). Moreover, results did not show any combination of compounds was more potent than compounds tested alone.

As such, there is insufficient evidence to suggest that an additive or synergistic effect influences the outcome of the bioassay. Furthermore, the treatments involving homarine and trigonelline, in combination with single compounds or mixtures (e.g., **2** + H + T, **4** + H + T), maintained the observed effects. However, none of these combinations were significantly different than the effect observed for homarine and trigonelline (H + T) or **2**, **4**, and **5** alone. In summary, the individual compound **4**, and all combinations, significantly increase shell strength compared to the uninduced control (SW), with combinations showing similar effects on increasing shell strength. This suggests that individual and combinatorial cue treatments similarly induce the oyster shell-strengthening responses (Figures 7-8).

3.4 Partially and tentatively annotated analytes of interest

The following mass spectral features corresponding to urinary metabolites of interest were only partially annotated, and candidate structures were not validated through comparison with authentic standards.

3.4.1 Structural analysis for metabolite with $[M+H]^+$ m/z 392.1602

Ethyl 4-[(*E*)-{[2,5-dimethyl-1-(3-nitrophenyl)-*1H*-pyrrol-3-yl]methylene}amino] benzoate (**7**) was proposed through mass spectral database matching for the metabolite whose molecular ion measured *m/z* 392.1602 (Table 3). Predicted by *in silico* MS fragmentation, 2-[4-(morpholine-4-carbonyl)-2-oxoquinolin-1-yl]-*N*-phenylacetamide (**8**), *N*-butyl-2-[4-[2-(4-nitroanilino)-2-oxoethyl]phenyl]acetamide (**9**), 3-(1,3-dioxoisoindol-2-yl)-*N*-[3-[(2-oxopyrrolidin-1-yl)methyl]phenyl]propenamide (**10**), *N*-[2-[[4-[(4-methylbenzoyl)amino]benzoyl]amino]ethyl]furan-2-carboxamide (**11**), *N*-(5-acetamido-2-methoxyphenyl)-1-benzyl-2-oxopyridine-3-carboxamide (**12**), exhibited Tanimoto similarity scores of 0.75, 0.35, 0.35, 0.30 and 0.34, respectively. Candidate structures associated with *m/z* 392.1602 are shown in Figure 9.

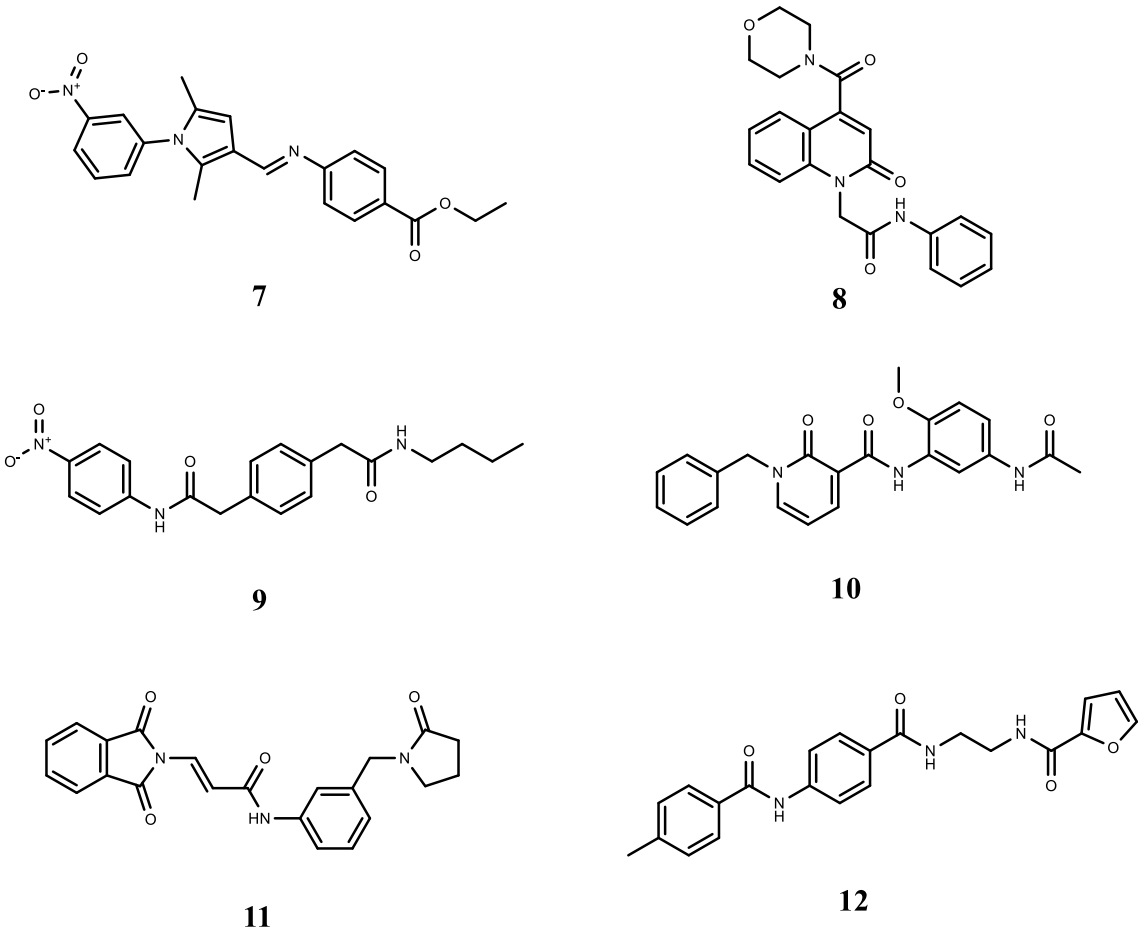

Figure 9: Candidate structures generated for the blue crab urine metabolite with $[M+H]^+$ *m/z* 392.1602 with a VIP score of 2.4 and a molecular formula of $C_{22}H_{21}N_3O_4$ including ethyl 4-[(*E*)-{[2,5-dimethyl-1-(3-nitrophenyl)-*1H*-pyrrol-3-yl]methylene}amino]benzoate (7) 2-[4-(morpholine-4-carbonyl)-2-oxoquinolin-1-yl]-N-phenylacetamide (8), N-butyl-2-[4-[2-(4-nitroanilino)-2-oxoethyl]phenyl]acetamide (9), 3-(1,3-dioxoisoindol-2-yl)-N-[3-[(2-oxopyrrolidin-1-yl)methyl]phenyl]propenamide (10), N-[2-[[4-[(4-methylbenzoyl)amino] benzoyl]amino]ethyl]furan-2-carboxamide (11), and N-(5-acetamido-2-methoxyphenyl)-1-benzyl-2-oxopyridine-3-carboxamide (12).

3.4.2 Structural analysis for metabolite with [M+H]⁺ m/z 230.1499

All candidate structures for the molecular feature with [M+H]⁺ *m/z* 230.1499 were predicted by *in silico* MS fragmentation including 3-acetamido-*N*-(3-acetamidopropyl)propenamide (**13**), *N*-(2-acetamidoethyl)-*N*'-butylethanediamide (**14**), 3-amino-*N*-(3-oxo-3-((3-oxobutyl)amino)propyl)propenamide (**15**), 2,6-diacetamidohexanamide (**16**), and 6-acetamido-*N*-(2-amino-2-oxoethyl)hexanamide (**17**) with Tanimoto similarity scores of 0.70, 0.66, 0.72, 0.63, and 0.66, respectively (Figure 10).

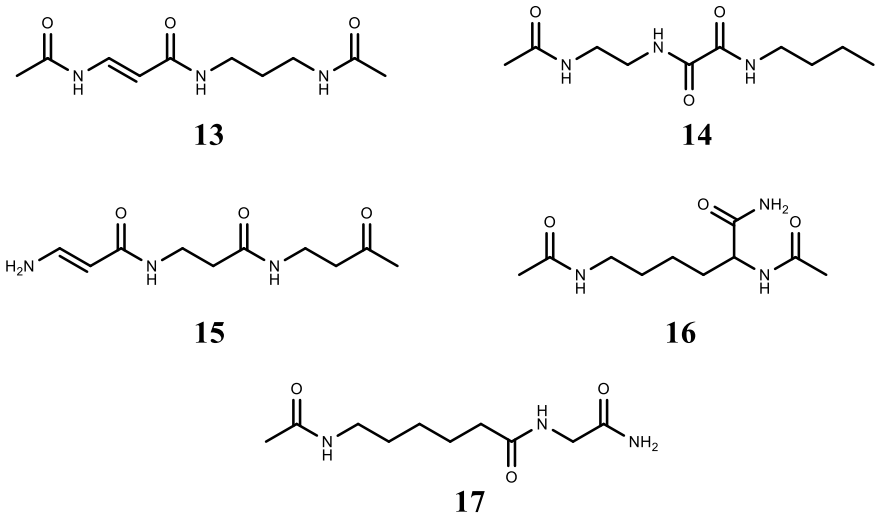

Figure 10: Candidate structures generated by *in silico* MS fragmentation for the blue crab urine metabolite with [M+H]⁺ *m/z* 230.1499 with a VIP score of 2.1 with the molecular formula $C_{10}H_{19}N_3O_3$: 3-acetamido-*N*-(3-acetamidopropyl)propenamide (13), *N*-(2-acetamidoethyl)-*N*'-butylethanediamide (14), 3-amino-*N*-(3-oxo-3-((3-oxobutyl)amino)propyl)propenamide (15), 2,6-diacetamidohexanamide (16), and 6-acetamido-*N*-(2-amino-2-oxoethyl)hexanamide (17).

As simple nitrogenous structures with modifications commonly found in nitrogenous waste products, **13**, **16**, and **17** are plausible candidates (Bender, 2012). It is reasonable that such compounds could result from the catabolism of amino acids or the breakdown of proteins. Candidate **14** is plausible but less so than **13**, **16**, and **17**, as the butyl group is hydrophobic and less typical in urinary excretions, which usually include more water-soluble compounds. Candidate **15** appears less plausible due to its structural simplicity.

3.4.3 Structural analysis for metabolite with $[M+H]^+$ m/z 250.0379

One candidate structure was considered for the metabolite with $[M+H]^+$ *m/z* 250.0379, with predicted molecular formula $C_8H_{11}NO_6S$. The VIP score calculated for this feature was 1.6 (Cepeda 2023). The candidate structure identified for this feature was 4-[(1*R*)-2-amino-1-hydroxyethyl]-2-hydroxyphenyl hydrogen sulfate (**18**) (Figure 11).

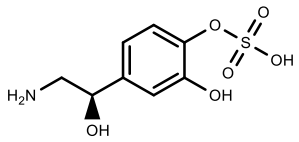

18

Figure 11: Candidate structure generated by *in silico* MS fragmentation for the blue crab urine metabolite with $[M+H]^+$ *m/z* 250.0379 with a VIP score of 1.6 with the molecular formula $C_8H_{11}NO_6S$: 4-[(1*R*)-2-amino-1-hydroxyethyl]-2-hydroxyphenyl hydrogen sulfate (18).

Candidate **18** is a likely candidate as its structure includes an aromatic ring with an amino-hydroxyethyl substituent and a sulfate group. The amino-hydroxyethyl side chain could be derived from amino acid metabolism associated with tyrosine, making it a plausible component of nitrogenous waste (Çakmak et al., 2020). The sulfate moiety is

significant as sulfation is common to the detoxification and excretion mechanisms observed in marine organisms (Kellner Filho et al., 2019). Additionally, this modification increases compounds' solubility in water, facilitating its removal through excretion.

3.4.4 Structural analysis for metabolite with $[M+H]^+$ m/z 269.1384

The candidate structure identified through database matching for the molecular ion with an *m/z* of 269.1384 was 2,5,8,11,14-pentaoxabicyclo[13.4.0]nonadeca-1(19),15,17-triene (**19**) (Table 3). The molecular structure of **19** is listed below (Figure 12).

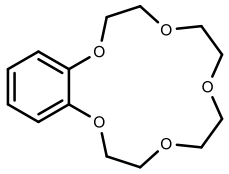

19

Figure 12: Candidate structure generated by MS fragmentation database matching for the blue crab urine metabolite with an $[M+H]^+$ *m/z* 269.1384, a VIP score of 1.5, and the molecular formula $C_{14}H_{20}O_5$: 2,5,8,11,14-pentaoxabicyclo[13.4.0]nonadeca-1(19),15,17-triene (19).

Candidate **19** is highly unlikely to be a natural excretory product due to the large and complex macrocyclic ether uncommon in biological compounds. Additionally, the multiple ether linkages and a hydrophobic macrocycle are not likely to be components of aqueous waste. Normal urinary excretions are small and water-soluble molecules that polar functional groups often modify to facilitate excretion in an aqueous environment (Benet et al, 1996). Without such polar groups, **19** is not likely to be a natural excretory product of blue crabs.

3.4.5 Structural analysis for metabolite with $[M+H]^+$ m/z 243.1340

One candidate structure, 5-ethyl-5-(4-hydroxy-2-pentanyl)-2,4,6(*1H,3H,5H*)-pyrimidinetrione (**20**), was tentatively annotated for the molecular ion with an *m/z* of 243.1340 having an associated VIP score of 1.5 (Cepeda 2023) (Figure 13).

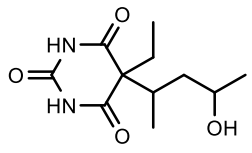

20

Figure 13: The candidate structure for 5-ethyl-5-(4-hydroxy-2-pentanyl)-2,4,6(*1H,3H,5H*)-pyrimidinetrione (20) (stereochemistry not defined) generated *in silico* for the molecular ion *m/z* 243.1340 with a VIP score of 1.5 with the molecular formula $C_{11}H_{18}N_2O_4$.

Candidate **20** is highly unlikely to be a natural component of blue crab urine having a pyrimidinetrione core and a ring system with three carbonyl groups, structural features uncommon to natural products. Pyrimidines are commonly found in biological molecules such as nucleotides, but the heavily oxidized form of pyrimidinetriones is not (Sui et al, 2021). The biosynthesis of candidate **20** would require specialized pathways that were not found in literature, suggesting crustaceans may not have the enzymes necessary to construct this compound.

CHAPTER 4. DISCUSSION

4.1 Prey species detect a complex mixture of chemical cues

The aim of this study was to identify the structures and quantify the concentrations of specific metabolites in blue crab urine that are implicated in inducing oyster shell strengthening. A primary focus was placed on a metabolite with a molecular weight 154.17 atomic mass units (AMU) and molecular formula $C_7H_{10}N_2O_2$, identified as the most important factor in explaining oyster shell strengthening models, as indicated by its high VIP scores (Cepeda, 2023). The metabolite was identified as 3-(1-methyl-*1H*-imidazol-4-yl)propanoic acid (**4**) (Figure 1), aligning with the MS^2 fragmentation patterns (Table 2, Table3), UPLC retention times (Figure 4), and ^1H NMR spectra observed for blue crab urine (Figure 3, Figure 4).

Compound **4** is biologically active in other organisms, exhibiting selective binding affinity to specific GABA receptors (Kisher-Hack et al., 2016). The concentration of this metabolite varied significantly (0.28 ∓ 0.49 µM in blue crab urine fed oysters and 0.12 ∓ 0.14 µM), with approximately half of the urine samples analyzed having no measurable amounts of this metabolites regardless of whether the blue crabs ate oysters or mud crabs prior to urine collection (Table 5). These concentrations are lower than those of homarine (13 ± 21 µM) and trigonelline (3.6 ± 6.9 µM), previously identified as relevant to oyster shell strengthening from blue crab urine (Roney et al., 2023). Another metabolite, *N*-acetylglucosamino-1,5-lactone also identified in blue crab urine, was observed at 0 µM to 50 µM, also generally higher than **4** (Kamio et al., 2014). In the current study, the observed concentration variation of **4** is likely to underrepresent the actual natural variation of the

metabolite in blue crab urine since samples measured in this study involved pooling urine from multiple individual blue crabs. Regardless, **4** appears to be present at lower concentrations than the few compounds previously quantified in blue crab urine (Poulin et al., 2018).

The blue crab urinary metabolites homarine and trigonelline have previously been shown to induce oyster shell strengthening and reduce mud crab foraging behavior (Poulin et al, 2018; Cepeda, 2023). Although these molecules were not among the top 10 features most significant from multivariate statistical models explaining oyster shell strengthening data (Cepeda, 2023), they induced oyster shell strengthening at levels similar to other treatment groups (Figure 6). Treatments in which homarine and trigonelline were combined with **2**, **4**, or **5** produced similar shell-strengthening responses in a non-specific manner. Since oysters rely exclusively on their shells for protection from predators, it is adaptive for them to exhibit a broad, binary shell-strengthening response (Pianka, 1970). This implies that oysters strengthen their shells in response to predator presence, regardless of predator identity (Bishop & Peterson 2006). Furthermore, the response observed to **2**, **4**, and **5**, with **2** and **5** not being components of blue crab urine, indicates the induced shell-strengthening response is not so specific that only individual molecules induce it. However, this is expected as receptor-ligand binding interactions have varying degrees of specificity, and the structural similarities of **2**, **4**, and **5** suggest that they may be expected to bind with the same receptor.

Prior literature has documented oysters' response to various predators, including mud crabs, oyster drills, and blue crabs (Roney et al., 2023; Ponce et al., 2020; Poulin et al., 2018; Scherer and Smee, 2017; Weissburg et al., 2016). As an oyster shell makes an

effective defense against many kinds predators, it seems intuitively reasonable for oysters' response to predators to be non-specific. By investing in a broadly useful defense, oysters maximize their defensive returns. Alternatively, investing energy into detecting and responding to a particular predator could decrease their available energy to invest into defenses useful against most predator species (Matsuda & Abrams, 2004).

Oysters, as sessile organisms, have limited options for defense compared to motile organisms. Oysters likely offset their high mortality rates through reproductive output, along with the ability to respond to general chemical cues from a variety predators, as supported by this thesis. Without the ability to detect predators, they would exhibit weaker shells and higher losses to predation (Bishop & Peterson 2006). The generalized response of oysters to multiple predator urinary metabolites suggests that oysters may not invest significant energy or resources in distinguishing or tailoring their responses to different combinations of predator-associated cues. Instead, they respond to various chemical cues, as demonstrated in this study (Figure 6) and in previously published literature (Scherer et al., 2016; Roney et al., 2023).

4.2 Induced oyster shell strengthening to facilitate oyster reef restoration.

The degradation of oyster reef habitat and the decline of oyster populations in the United States are multifaceted issues. As such, no single solution is likely to completely reverse these trends. The results of the current study and previously reported increased survival of 58% among oyster spat exposed to blue crab cues suggest that exposure to these chemical cues will reduce oyster mortality due to predation (Figure 6) (Scherer et al.,

2017). However, spat survival will be influenced by the location of spat settlement and the different predators in that location (Belgrad et al., 2023).

Inducing oyster shell strengthening in oyster hatcheries using chemical cues may produce stronger oyster spat more resistant to predation. Applying such cues in a hatchery setting could be controlled so that the chemicals would not enter the open ocean (Kamermans et al., 2017; Belgrad et al., 2021). In this way, these chemical cues may reduce oyster mortality due to predation without impacting the broader environment. The controlled application of chemical cues, such as the metabolite identified in the current study, is likely to positively impact the survival of oyster spat. A method that allows for the controlled and scalable application of cues such as **4**, homarine, and trigonelline on newly settled oyster spat, would mitigate the effect of predation on the mortality of hatchery-reared oysters (Kennedy et al., 2011). However, additional research should investigate the potential ecological impact of incorporating these cues in hatchery settings.

4.3 Metabolomics as a tool for identifying natural products.

This study provides context on oysters' (*C. virginica*) ability to detect and respond to various structurally similar chemical cues and highlights the usefulness of metabolomic methods for identifying metabolites important in ecological interactions (Kellog & Kang 2020; Liu et al., 2021; Bayona et al., 2022). When performed on untargeted metabolomics datasets, regression analyses such as partial least-squared regression analyses enable the correlation of chemical composition with biological data (Poulin et al, 2018; Cepeda, 2023). Advances in machine learning algorithms and expanding spectral datasets have further enhanced the feasibility of identifying unknown compounds from complex

biological mixtures when paired with appropriate biological data. Tools like SIRIUS and CSI:FingerID allow specific fragment ion patterns to be proposed for with molecular substructures via *in silico* predictions, even for compounds for which no MS data are available. Applying such tools with state-of-the-art ^{1}H NMR spectral analysis tools such as SAND will allow researchers to identify individual NMR signals in a complex mixture with significantly greater accuracy and speed than was previously possible (Wu et al. 2024).

Future investigations should seek to develop regression models and assign VIP scores for both the molecular features and ^{1}H NMR signals in complex samples deconvoluted using the Spectral Automated NMR Decomposition (SAND) model (Wu et al, 2024). Doing so allows ^{1}H NMR signals to be associated with a corresponding mass spectral feature through their identical VIP scores. Such applications would eliminate the necessity of purifying or fractionating chemically complex samples, allowing for the rapid and accurate identification of unknown compounds. Applying these data manipulation techniques would contribute directly to chemical cue and drug discovery efforts and greatly contribute to the fields of metabolomics and chemical ecology.

Similarly, this study advances the fields of metabolomics, chemical ecology, and oyster restoration efforts by identifying chemical cues that modulate predator-prey interactions between blue crabs and oysters. Although the ecological and commercial importance of such cues is apparent, the majority of the individual molecules that make up complex chemical cues remain unidentified – especially for inducible waterborne defenses (Poulin et al., 2018; Roney et al., 2023). The techniques described herein, which used PLS-R models to identify molecular features important for ecological outcomes, can be

incorporated into any investigation in which there is variation among chemically complex samples and quantitative information on biological responses. The structural elucidation of resultant molecular features can be achieved by matching daughter MS fragments to ever-expanding mass spectrometry databases, and advanced AI-driven structure prediction techniques.

This study's findings shed light on oysters' ability to detect and respond to various structurally similar chemical cues. While oysters do detect and respond to chemical cues, the detection of chemical cues is not highly selective for individual cues, as can be seen by the induction of **2**, **4**, **5**, homarine, and trigonelline (Figure 6, Figure 7) (Cepeda et al., 2023; Roney et al., 2023). Moreover, there was no evidence that oysters differentiate between individual and combinations of chemical cues supporting their shell-strengthening response to be more general than highly specific. This may result from the structural similarities of **2**, **4**, **5**, and of homarine and trigonelline. Future investigations should identify the receptor(s) and binding affinity of these compounds with their receptor, which would allow for a deeper understanding of the mechanism for oyster shell strengthening.

REFERENCES

Aires-de-Sousa, J., Hemmer, M., & Gasteiger, J. (2002). Prediction of 1H NMR chemical shifts using neural networks. *Analytical Chemistry*, *74*(1), 80–90.

Aletor, V. A., & Onibi, O. E. (1990). Use of oyster shell as calcium supplement. Part 1. Effect on the utilization of gossypol-containing cotton seed cake by the chicken. *Food / Nahrung*, *34*(4), 311–318. https://doi.org/10.1002/food.19900340403

Anderson, T. H., & Taylor, G. T. (2001). Nutrient Pulses, Plankton Blooms, and Seasonal Hypoxia in Western Long Island Sound. *Estuaries*, *24*(2), 228. https://doi.org/10.2307/1352947

Baldwin, I. T. (1998). Jasmonate-induced responses are costly but benefit plants under attack in native populations. *Proceedings of the National Academy of Sciences*, *95*(14), 8113–8118. https://doi.org/10.1073/pnas.95.14.8113

Banfi, D., & Patiny, L. (2008). Www. Nmrdb. Org: Resurrecting and processing NMR spectra on-line. *Chimia*, *62*(4), 280–280.

Bartol, I. K., Mann, R., & Luckenbach, M. (1999). Growth and mortality of oysters (Crassostrea virginica) on constructed intertidal reefs: Effects of tidal height and substrate level. *Journal of Experimental Marine Biology and Ecology*, *237*(2), 157–184. https://doi.org/10.1016/S0022-0981(98)00175-0

Bayona, L. M., De Voogd, N. J., & Choi, Y. H. (2022). Metabolomics on the study of marine organisms. *Metabolomics*, *18*(3), 17. https://doi.org/10.1007/s11306-022-01874-y

Beck, M. W., Brumbaugh, R. D., Airoldi, L., Carranza, A., Coen, L. D., Crawford, C., Defeo, O., Edgar, G. J., Hancock, B., Kay, M. C., Lenihan, H. S., Luckenbach, M. W., Toropova, C. L., Zhang, G., & Guo, X. (2011). Oyster Reefs at Risk and Recommendations for Conservation, Restoration, and Management. *BioScience*, *61*(2), 107–116. https://doi.org/10.1525/bio.2011.61.2.5

Belgrad, B. A., Combs, E. M., Walton, W. C., & Smee, D. L. (2021). Use of predator cues to bolster oyster resilience for aquaculture and reef restoration. *Aquaculture*, *538*, 736553. https://doi.org/10.1016/j.aquaculture.2021.736553

Belgrad, B. A., Smee, D. L., & Weissburg, M. J. (2023). Predator signaling of multiple prey on different trophic levels structures trophic cascades. *Ecology*, *104*(6), e4050. https://doi.org/10.1002/ecy.4050

Bender, D. (2012). *Amino Acid Metabolism.* Wiley.

Benet, L., Kroetz, D., Sheiner, L., Hardman, J., & Limbird, L. (1996). Pharmacokinetics: The dynamics of drug absorption, distribution, metabolism, and elimination. In *Goodman and Gilman's the pharmacological basis of therapeutics* (e27 ed., Vol. 3).

Bishop, M. J., & Peterson, C. H. (2006). When *r* -Selection May Not Predict Introduced-Species Proliferation: Predation Of A Nonnative Oyster. *Ecological Applications*, *16*(2), 718–730. https://doi.org/10.1890/1051-0761(2006)016[0718:WRMNPI]2.0.CO;2

Booth, H., Pusack, T., White, J., Stallings, C., & Kimbro, D. (2018). Intraspecific predator inhibition, not a prey size refuge, enables oyster population persistence during

predator outbreaks. *Marine Ecology Progress Series*, *602*, 155–167. https://doi.org/10.3354/meps12704

Brönmark, C., & Miner, J. (1992). Predator-induced phenotypical change in body morphology in crucian carp. 258:1348–1350 Carr WES, Netherton JC III, Gleeson RA, Derby CD (1996) Stimulants. *Science*, *258*, 1348–1350.

Burreson, E., & Ragone Calvo, L. (1996). Epizootiology of Perkinsus marinus disease of oysters in Chesapeake Bay, with emphasis on data since 1985. *Journal of Shellfish Research*, *15*(1), 17–34.

Buzan, D., Weber, K., Rodney, B., & Legare, B. (2015). SAVING BURIED OYSTERS. *Proceedings of Western Dredging Association and Texas A&M University Center for Dredging Studies*, *22–25*.

Çakmak, O., Ökten, S., Alımlı, D., Ersanlı, C. C., Taslimi, P., & Koçyiğit, Ü. M. (2020). Novel piperazine and morpholine substituted quinolines: Selective synthesis through activation of 3,6,8-tribromoquinoline, characterization and their some metabolic enzymes inhibition potentials. *Journal of Molecular Structure*, *1220*, 128666. https://doi.org/10.1016/j.molstruc.2020.128666

Carroll, J., Marion, J., & Finelli, C. (2015). A field test of the effects of mesopredators and landscape setting on juvenile oyster, Crassostrea virginica, consumption on intertidal reefs. *Marine Biology*, *162*, 993–1003.

Castillo, A., Patiny, L., & Wist, J. (2011). Fast and accurate algorithm for the simulation of NMR spectra of large spin systems. *Journal of Magnetic Resonance*, *209*(2), 123–130.

Cepeda, M. (2023). *An exploration of chemical cues as mediators of marine predator-prey interactions* [Georgia Institute of Technology]. https://hdl.handle.net/1853/75591

Coen, L., Luckenbach, M., & Breitburg, D. (1999). The Role of Oyster Reefs as Essential Fish Habitat: A Review of Current Knowledge and Some New Perspectives. *American Fisheries Society Symposium*, *22*.

Cronin, G., & Hay, M. E. (1996). Induction of Seaweed Chemical Defenses by Amphipod Grazing. *Ecology*, *77*(8), 2287–2301. https://doi.org/10.2307/2265731

Dame, R., John, S., & Thomas, W. (1989). *Carbon, nitrogen and phosphorus processing by an oyster reef*. 249–256.

Davis, H. (1958). Survival and growth of clam and oyster larvae at different salinities. *The Biological Bulletin*, *114*(3), 296–307.

Dugas, R., Edwin, J., & Berrigan, M. (1997). History and Status of the Oyster, Crassostrea virginica, and Other Molluscan Fisheries of the U.S. Gulf of Mexico. *NOAA Technical Report NMFS*, *1*, 187–210.

Dunstan, R. H., Sparkes, D. L., Macdonald, M. M., De Jonge, X. J., Dascombe, B. J., Gottfries, J., Gottfries, C.-G., & Roberts, T. K. (2017). Diverse characteristics of the urinary excretion of amino acids in humans and the use of amino acid supplementation to reduce fatigue and sub-health in adults. *Nutrition Journal*, *16*(1), 19. https://doi.org/10.1186/s12937-017-0240-y

Editorial: Childhood poisoning: prevention and first-aid management. (1975). *British Medical Journal*, *4*(5995), 483–484. https://doi.org/10.1136/bmj.4.5995.483

Flowers, G. J. L., Needham, H. R., Bulmer, R. H., Lohrer, A. M., & Pilditch, C. A. (2024). The Effect of Sediment Mud Content on Primary Production in Seagrass and

Unvegetated Intertidal Flats. *Estuaries and Coasts*, *47*(6), 1544–1560. https://doi.org/10.1007/s12237-024-01403-1

Grabowski, J. H., Brumbaugh, R. D., Conrad, R. F., Keeler, A. G., Opaluch, J. J., Peterson, C. H., Piehler, M. F., Powers, S. P., & Smyth, A. R. (2012). Economic Valuation of Ecosystem Services Provided by Oyster Reefs. *BioScience*, *62*(10), 900–909. https://doi.org/10.1525/bio.2012.62.10.10

Hallegraeff, G. (2003). Harmful algal blooms: A global overview. *Manual on Harmful Marine Microalgae*, *33*, 1–22.

Harrison, W., Lynch, M., & Altschaeffl, A. (1964). Sediments of lower Chesapeake Bay, with emphasis on mass properties. *Journal of Sedimentary Research*, *34*(4), 727–755.

Hay, M. E. (2009). Marine Chemical Ecology: Chemical Signals and Cues Structure Marine Populations, Communities, and Ecosystems. *Annual Review of Marine Science*, *1*(1), 193–212. https://doi.org/10.1146/annurev.marine.010908.163708

Hessen, D. O., & Van Donk, E. (n.d.). Morpholigical changes in Scenedesmus induced by substances released from Daphnia. *Archiv Für Hydrobiologie*, *127*, 129–140.

Horiguchi, I., Mimura, Y., & Monteiro, P. J. M. (2021). Plant-growing performance of pervious concrete containing crushed oyster shell aggregate. *Cleaner Materials*, *2*, 100027. https://doi.org/10.1016/j.clema.2021.100027

Hutchings, P., & Recher, H. (1984). The fauna of Careel Bay with comments on the ecology of mangrove and sea-grass communities. *Australian Zoology*, *18*, 99–128.

Jesse, J. A., Agnew, M. V., Arai, K., Armstrong, C. T., Hood, S. M., Kachmar, M. L., Long, J. T., McCarty, A. J., Ross, M. O., Rubalcava, K. D., Shaner, J., Tanaka, S.,

Wood, L., Schott, E. J., & Wilberg, M. J. (2021). Effects of Infectious Diseases on Population Dynamics of Marine Organisms in Chesapeake Bay. *Estuaries and Coasts*, *44*(8), 2334–2349. https://doi.org/10.1007/s12237-021-00915-4

Johansson, N., & Granéli, E. (1999). Influence of different nutrient conditions on cell density, chemical composition and toxicity of Prymnesium parvum (Haptophyta) in semi-continuous cultures. *Journal of Experimental Marine Biology and Ecology*, *239*(2), 243–258. https://doi.org/10.1016/S0022-0981(99)00048-9

Jørgensen, B. (n.d.). Bivalve filter feeding revisited. *Marine Ecology Progress Series*, *142*, 287–302.

Kamermans, P., Blanco, A., Joaquim, S., Matias, D., Magnesen, T., Nicolas, J. L., Petton, B., & Robert, R. (2016). Recirculation nursery systems for bivalves. *Aquaculture International*, *24*(3), 827–842. https://doi.org/10.1007/s10499-016-9990-3

Kamio, M., Schmidt, M., Germann, M. W., Kubanek, J., & Derby, C. D. (2013). The smell of moulting: *N* -acetylglucosamino-1,5-lactone is a premoult biomarker and candidate component of the courtship pheromone in the urine of the blue crab, *Callinectes sapidus*. *Journal of Experimental Biology*, jeb.099051. https://doi.org/10.1242/jeb.099051

Kaspar, H., Gillespie, P., Boyer, I., & MacKenzie, A. (1985). Effects of mussel aquaculture on the nitrogen cycle and benthic communities in Kenepuru Sound, Marlborough Sounds, New Zealand. *Marine Biology*, *85*, 127–136.

Kellner Filho, L. C., Picão, B. W., Silva, M. L. A., Cunha, W. R., Pauletti, P. M., Dias, G. M., Copp, B. R., Bertanha, C. S., & Januario, A. H. (2019). Bioactive Aliphatic

Sulfates from Marine Invertebrates. *Marine Drugs*, *17*(9), 527. https://doi.org/10.3390/md17090527

Kellogg, J., & Kang, S. (2020). Metabolomics, an Essential Tool in Exploring and Harnessing Microbial Chemical Ecology. *Phytobiomes Journal*, *4*(3), 195–210. https://doi.org/10.1094/PBIOMES-04-20-0032-RVW

Kennedy, V. S., Breitburg, D. L., Christman, M. C., Luckenbach, M. W., Paynter, K., Kramer, J., Sellner, K. G., Dew-Baxter, J., Keller, C., & Mann, R. (2011). Lessons Learned from Efforts to Restore Oyster Populations in Maryland and Virginia, 1990 to 2007. *Journal of Shellfish Research*, *30*(3), 719–731. https://doi.org/10.2983/035.030.0312

Lima, S. L. (1998). Nonlethal Effects in the Ecology of Predator-Prey Interactions. *BioScience*, *48*(1), 25–34. https://doi.org/10.2307/1313225

Liu, R., Bao, Z.-X., Zhao, P.-J., & Li, G.-H. (2021). Advances in the Study of Metabolomics and Metabolites in Some Species Interactions. *Molecules*, *26*(11), 3311. https://doi.org/10.3390/molecules26113311

Mann, R., & Powell, E. N. (2007). WHY OYSTER RESTORATION GOALS IN THE CHESAPEAKE BAY ARE NOT AND PROBABLY CANNOT BE ACHIEVED. *Journal of Shellfish Research*, *26*(4), 905–917. https://doi.org/10.2983/0730-8000(2007)26[905:WORGIT]2.0.CO;2

Matsuda, H., & Abrams, P. (2004). Effects of predator prey interactions and adaptive change on sustainable yield. *Canadian Journal of Fisheries and Aquatic Sciences*, *61*(2), 175–184.

Minello, T. (1999). Nekton densities in shallow estuarine habitats of Texas and Louisiana and the identification of essential fish habitat. *In American Fisheries Society Symposium*, *22*, 43–75.

Morton, R., Miller, T., & Moore, L. (2005). Historical Shoreline Changes along the US Gulf of Mexico: A Summary of Recent Shoreline Comparisons and Analyses. *Journal of Coastal Research*, *21*(4), 704–709.

Nestlerode, J. A., Luckenbach, M. W., & O'Beirn, F. X. (2007). Settlement and Survival of the Oyster *Crassostrea virginica* on Created Oyster Reef Habitats in Chesapeake Bay. *Restoration Ecology*, *15*(2), 273–283. https://doi.org/10.1111/j.1526-100X.2007.00210.x

Orth, R. J., Heck, K. L., & Van Montfrans, J. (1984). Faunal Communities in Seagrass Beds: A Review of the Influence of Plant Structure and Prey Characteristics on Predator: Prey Relationships. *Estuaries*, *7*(4), 339. https://doi.org/10.2307/1351618

Patiny, L., Musallam, H., Bolaños, A., Zasso, M., Wist, J., Karayilan, M., & Schlörer, N. (2024). NMRium: Teaching nuclear magnetic resonance spectra interpretation in an online platform. *Beilstein Journal of Organic Chemistry*, *20*(1), 25–31.

Pease, S. K. D., Brosnahan, M. L., Sanderson, M. P., & Smith, J. L. (2022). Effects of Two Toxin-Producing Harmful Algae, Alexandrium catenella and Dinophysis acuminata (Dinophyceae), on Activity and Mortality of Larval Shellfish. *Toxins*, *14*(5), 335. https://doi.org/10.3390/toxins14050335

Pianka, E. (1970). On r-and K-selection. *The American Naturalist*, *104*(904), 592–597.

Ponce, M., Belgrad, B., Walton, W., & Smee, L. (2020). Nursery Exposure of Oyster Spat to Different Predators Strengthens Oyster Shells. *Gulf and Caribbean Research*, *31*, SC36–SC40. https://doi.org/10.18785/gcr.3101.14

Poulin, R. X., Lavoie, S., Siegel, K., Gaul, D. A., Weissburg, M. J., & Kubanek, J. (2018). Chemical encoding of risk perception and predator detection among estuarine invertebrates. *Proceedings of the National Academy of Sciences*, *115*(4), 662–667. https://doi.org/10.1073/pnas.1713901115

Roegner, C., & Mann, R. (1995). Early Recruitment and Growth of the American Oyster Crassostrea Virginica (Bivalvia: Ostreidae) with Respect to Tidal Zonation and Season. *Marine Ecology Progress Series*, *117*(1/3), 91–101.

Roney, S. H., Cepeda, M. R., Belgrad, B. A., Moore, S. G., Smee, D. L., Kubanek, J., & Weissburg, M. J. (2023). Common fear molecules induce defensive responses in marine prey across trophic levels. *Oecologia*, *202*(4), 655–667. https://doi.org/10.1007/s00442-023-05438-2

Scavia, D., Field, J. C., Boesch, D. F., Buddemeier, R. W., Burkett, V., Cayan, D. R., Fogarty, M., Harwell, M. A., Howarth, R. W., Mason, C., Reed, D. J., Royer, T. C., Sallenger, A. H., & Titus, J. G. (2002). Climate change impacts on U.S. Coastal and Marine Ecosystems. *Estuaries*, *25*(2), 149–164. https://doi.org/10.1007/BF02691304

Schatz, A., McDowell, J., Biesack, E. E., & Rivest, E. B. (2024). Relative importance of phenotypic plasticity and carryover effects in response to small salinity shifts during oyster aquaculture production. *Aquaculture*, *581*, 740432. https://doi.org/10.1016/j.aquaculture.2023.740432

Scherer, A. E., Bird, C. E., McCutcheon, M. R., Hu, X., & Smee, D. L. (2018). Two-tiered defense strategy may compensate for predator avoidance costs of an ecosystem engineer. *Marine Biology*, *165*(8), 131. https://doi.org/10.1007/s00227-018-3391-2

Scherer, A. E., Lunt, J., Draper, A. M., & Smee, D. L. (2016). Phenotypic plasticity in oysters (*Crassostrea virginica*) mediated by chemical signals from predators and injured prey. *Invertebrate Biology*, *135*(2), 97–107. https://doi.org/10.1111/ivb.12120

Scherer, A. E., & Smee, D. L. (2017). Eastern Oysters *Crassostrea virginica* Produce Plastic Morphological Defenses in Response to Crab Predators Despite Resource Limitation. *The Biological Bulletin*, *233*(2), 144–150. https://doi.org/10.1086/695470

Schmitz, O. J. (2008). Effects of Predator Hunting Mode on Grassland Ecosystem Function. *Science*, *319*(5865), 952–954. https://doi.org/10.1126/science.1152355

Selander, E., Kubanek, J., Hamberg, M., Andersson, M. X., Cervin, G., & Pavia, H. (2015). Predator lipids induce paralytic shellfish toxins in bloom-forming algae. *Proceedings of the National Academy of Sciences*, *112*(20), 6395–6400. https://doi.org/10.1073/pnas.1420154112

Smayda, T. J. (2008). Complexity in the eutrophication–harmful algal bloom relationship, with comment on the importance of grazing. *Harmful Algae*, *8*(1), 140–151. https://doi.org/10.1016/j.hal.2008.08.018

Smee, D. L., & Weissburg, M. J. (2006). CLAMMING UP: ENVIRONMENTAL FORCES DIMINISH THE PERCEPTIVE ABILITY OF BIVALVE PREY.

Ecology, *87*(6), 1587–1598. https://doi.org/10.1890/0012-9658(2006)87[1587:CUEFDT]2.0.CO;2

Stearns, S. (1976). Life-history tactics: A review of the ideas. *The Quarterly Review of Biology*, *51*(1), 3–47.

Stifel, F. B., & Herman, R. H. (1971). Histidine metabolism. *The American Journal of Clinical Nutrition*, *24*(2), 207–217. https://doi.org/10.1093/ajcn/24.2.207

Sui, Y., Ansari, M. F., & Zhou, C. (2021). Pyrimidinetrione-imidazoles as a Unique Structural Type of Potential Agents towards *Candida Albicans*: Design, Synthesis and Biological Evaluation. *Chemistry – An Asian Journal*, *16*(11), 1417–1429. https://doi.org/10.1002/asia.202100146

Tack, J. F., & Polk, P. (1996). The Uptake of Colloidal Melanin from Seawater by Marine Bivalves. *Marine Ecology*, *17*(1–3), 543–548. https://doi.org/10.1111/j.1439-0485.1996.tb00526.x

Thomsen, M. S., & McGlathery, K. (2006). Effects of accumulations of sediments and drift algae on recruitment of sessile organisms associated with oyster reefs. *Journal of Experimental Marine Biology and Ecology*, *328*(1), 22–34. https://doi.org/10.1016/j.jembe.2005.06.016

Thrush, S., & Dayton, P. (2002). Disturbance to Marine Benthic Habitats by Trawling and Dredging: Implications for Marine Biodiversity. *Annual Review of Ecology and Systematic*, *33*, 449–473. http://www.jstor.org/stable/3069270

Tice-Lewis, M., Zhang, Y. S., Redding, S. G., Lindquist, N. L., Rodriguez, A. B., Fieseler, C. M., Walker, Q. A., & Fodrie, F. J. (2022). Coastal squeeze on temperate reefs:

Long-term shifts in salinity, water quality, and oyster-associated communities. *Ecological Applications*, *32*(5), e2609. https://doi.org/10.1002/eap.2609

Turner, R. (1977). Intertidal vegetation and commercial yields of penaeid shrimp. *Transactions of the American Fisheries Society*, *106*(5), 411–416.

Volety, A. K. (2008). Effects of salinity, heavy metals and pesticides on health and physiology of oysters in the Caloosahatchee Estuary, Florida. *Ecotoxicology*, *17*(7), 579–590. https://doi.org/10.1007/s10646-008-0242-9

Weissburg, M., Poulin, R. X., & Kubanek, J. (2016). You Are What you Eat: A Metabolomics Approach to Understanding Prey Responses to Diet-Dependent Chemical Cues Released by Predators. *Journal of Chemical Ecology*, *42*(10), 1037–1046. https://doi.org/10.1007/s10886-016-0771-2

Weng, N., & Wang, W.-X. (2019). Seasonal fluctuations of metal bioaccumulation and reproductive health of local oyster populations in a large contaminated estuary. *Environmental Pollution*, *250*, 175–185. https://doi.org/10.1016/j.envpol.2019.04.019

Werner, E. E., & Gilliam, J. F. (1984). The Ontogenetic Niche and Species Interactions in Size-Structured Populations. *Annual Review of Ecology and Systematics*, *15*(1), 393–425. https://doi.org/10.1146/annurev.es.15.110184.002141

Wilberg, M., Livings, M., Barkman, J., Morris, B., & Robinson, J. (2011). Overfishing, disease, habitat loss, and potential extirpation of oysters in upper Chesapeake Bay. *Marine Ecology Progress Series*, *436*, 131–144. https://doi.org/10.3354/meps09161

Wu, Y., Sanati, O., Uchimiya, M., Krishnamurthy, K., Wedell, J., Hoch, J. C., Edison, A. S., & Delaglio, F. (2024a). SAND: Automated Time-Domain Modeling of NMR Spectra Applied to Metabolite Quantification. *Analytical Chemistry*, acs.analchem.3c03078. https://doi.org/10.1021/acs.analchem.3c03078

Wu, Y., Sanati, O., Uchimiya, M., Krishnamurthy, K., Wedell, J., Hoch, J. C., Edison, A. S., & Delaglio, F. (2024b). SAND: Automated Time-Domain Modeling of NMR Spectra Applied to Metabolite Quantification. *Analytical Chemistry*, *96*(5), 1843–1851. https://doi.org/10.1021/acs.analchem.3c03078

Yasumoto, K., Nishigami, A., Yasumoto, M., Kasai, F., Okada, Y., Kusumi, T., & Ooi, T. (2005). Aliphatic sulfates released from Daphnia induce morphological defense of phytoplankton: Isolation and synthesis of kairomones. *Tetrahedron Letters*, *46*(28), 4765–4767. https://doi.org/10.1016/j.tetlet.2005.05.027

Zimme-Faust, R., & Tamburri, M. (1994). Chemical identity and ecological implications of a waterborne, larval settlement cue. *Limnology and Oceanography*, *39*(5), 1075–1087.

Zu Ermgassen, P. S. E., Spalding, M. D., Blake, B., Coen, L. D., Dumbauld, B., Geiger, S., Grabowski, J. H., Grizzle, R., Luckenbach, M., McGraw, K., Rodney, W., Ruesink, J. L., Powers, S. P., & Brumbaugh, R. (2012). Historical ecology with real numbers: Past and present extent and biomass of an imperilled estuarine habitat. *Proceedings of the Royal Society B: Biological Sciences*, *279*(1742), 3393–3400. https://doi.org/10.1098/rspb.2012.0313